Using Hemispheric Sensing with Trajectory Prediction to Mechanically Dodge Space Debris

New Mexico

Supercomputing Challenge

Final Report

April 11th, 2021

Team #51

Albuquerque Institute for Mathematics and Science

Team Members

McKenna Collins

Teacher

Mr. Creighton Edington

Project Mentors

Dr. Thomas Peng

Mr. Creighton Edington

ABSTRACT

Space debris of any size can cause irreparable damage to multimillion-dollar satellites. Satellites typically dodge space debris via an orbital maneuver drawing from their finite fuel supply. However, this option can negatively affect length of the mission. However, new satellite systems could be divided into multiple subsections to perform mechanical orbital maneuvers and avoid space debris without propellant loss. This approach requires an onboard detection system with multiple sensors and corresponding algorithms capable of predicting the trajectory of localized space debris. In the best-case scenario, the satellite would be segmented, with its sections mechanically separated, allowing the detected space debris to pass through the more vacant center of mass. Afterwards, the total module would be reintegrated. To model the sequence described, seven prototypes were designed, built, and tested. Proof of concept for preliminary functionality was achieved in the first phase of the experimentation. The remaining prototypes were tested for separation distance, frequency of successful detection, and reintegration cycles. While the latest prototype is the most promising, it does require scaling up to a version that is capable of separation of parts to permit debris of several kilometers to pass through the system.

PROBLEM

The quantity of space debris in orbit has been increasing as more payloads are launched and existing cataloged objects collide with and fragment one another (Klinkrad, 2010). Some of this debris is from non-functional man-made objects, other include fragments from slag, or solidified alumina from motor fuel, and some waste originated from explosions or spacecraft collisions (Klinkrad, 2010). Additionally, smaller pieces of debris can potentially derive from paint chips (Commission on Engineering and Technical Systems, 1995). Irreparable damage to expensive equipment that enables a satellite's mission has been caused by miniscule pieces of space debris due to the high speeds found in orbit (Garcia, 2017).

Larger space debris is traceable from ground level, but smaller particles such as paint flecks often go untracked (Garcia, 2017). Programs like the Meteoroid and Space Debris Terrestrial Environment Reference (MASTER) can use mathematics to track space debris by using data from known events (Esa, 2018). The efforts to detect smaller debris from space and measure its impact velocity in the "Space Debris Sensor" experiment employed a localized detection range, but this experiment seemed to wait for a collision to occur in order to measure it (Cofield, 2017). Other efforts to predict the location of exploded space debris utilize velocity distribution models, however, tracking smaller individual debris can still present difficulties (Cavallaro, 2019).

According to the literature, at least two systems are required to protect satellites from small space debris. One system provides detection. The other, conjoined system functions to avoid space debris.

The detection system required should have a spherical field of view and be able to identify and calculate the trajectory path of space debris. To predict the trajectory path of an object, distance measurements and a trilateration algorithm can be used. A similar trajectory scheme was done in an indoor robot tracking experiment, where range sensors can apply a series of equations to determine the relative (x, y, z) coordinates of an object (Cotera et al, 2016) to obtain distance output data. The coordinates represent the position of an object in three-dimensional space relative to a predetermined origin. If two (x, y, z) coordinates are found at different time intervals, the location of the object in the future is predictable using the parametric equations derived from the two points (Maths Learning Centre of UofA, 2013). Using this data,

an onboard hemispherical sensing system can predict if space debris is going to collide with a designated spacecraft.

To minimize damage to space vehicles, current ground-based avoidance techniques require execution of traditional orbital maneuvers. However, to perform such a maneuver, satellites expend valuable propellant. While the short-term solution of depleting finite propellant supply to avoid imminent danger is a solution for safety, it is not optimal for prolonging the lifespan of the mission. Propellant is vital to keep a satellite operational. Without propellant, satellites are not able to counter gravitational drag over time or to stay in a certain position if needed for its mission (Bellatrix, 2015). Propellantless space operations have been previously designed, such as pyrotechnically detachable bolts (Cespedosa et al, 2000), but they still consume finite resources and are non-recoverable. However, a novel mechanical device can be designed to repeatedly enable a satellite to perform an orbital maneuver without propellant. This process can be performed by mechanically repelling sectionalized satellite segments away from one another, then tethering the parts together for post maneuver reintegration. This dual detection-avoidance system does not rely on either ground sensing or ground-to-satellite communications. This paper is arranged to describe the methodology and define the prototypes constructed and tested. Results, analysis, conclusions, and future work are also presented.

METHODS

General

Seven main prototypes were designed, built, and tested to achieve detection and avoidance of space debris for varying sizes of satellites, with current motions towards cube-sats. Each prototype followed the process from proof of concept to physical design and bench testing. The prototypes were built and tested modularly and as part of a functional system.

Phase I: Overall System Proof of Concept Design

The first prototype consisted of a Styrofoam ball cut in half, a three-dimensional (3D) printed pin latch for a spring, four ribbon tethers between the halves, a 3D printed tether guide, and a spring (Figure 1). This prototype was manually operated by compressing the spring inside
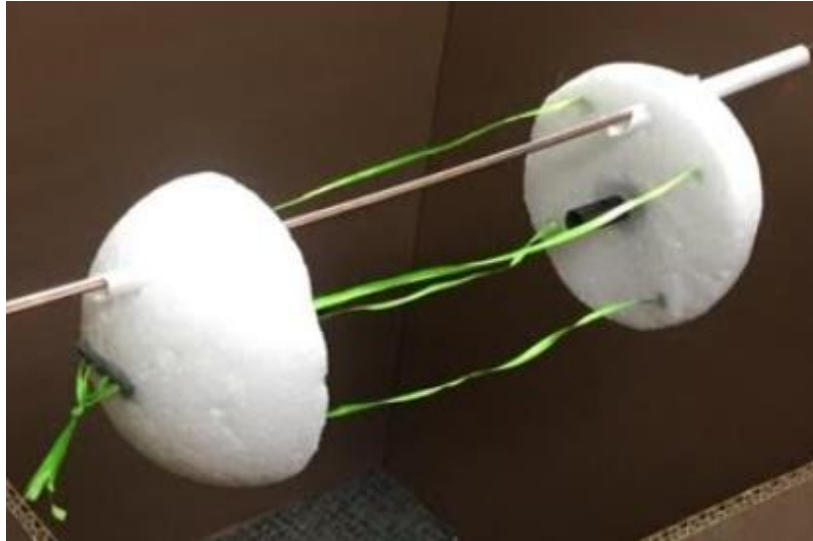
Figure 1: *Prototype 1.*

the latch system located between the two halves. The spring was released by manually pulling the pin in the latch. The tethers prevented the halves from completely flying away.

Phase II: Automated Tether Operation

To decrease human involvement in operating the system, the next phase of the experimental design was similarly structured with four string tethers. This time, a 3D printed body was used in combination with a direct current (DC) motor. The design included a spindle to manipulate the tethers and the motor was supposed to replace the latch (Figure 2).

Figure 2; *contents: Prototype 2*

Phase III: *Horizontal Clutch Design and Separating Mechanism Testing*

It became evident that more torque was required to wind tethers to completely compress a spring. The stand-alone DC motor proved inefficient. The latch was fabricated as a horizontal clutch (Figure 3). The system could then operate without tactile interference. To refine the separation system, both an electromagnet (Figure 4) and spring (Figure 5) separating system were installed.

Figure 3; *contents: Prototype 3*
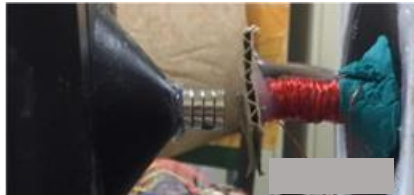
Figure 4; *contents: Electromagnet separating system*

Figure 5; *contents: Spring separating system*

This setup was run manually ten times. The two halves of the prototype were suspended from the ceiling to employ gravity for farther separation distances. Each trial was started by manually connecting a battery to each component in chronological order for a separation and reintegration maneuver. After separating, the distance the sections parted was measured to determine system effectiveness.

Phase IV: Use of Gears

In an attempt to build a stronger and ruggedized prototype, the phase four prototype (Figure 6) employed a similar horizontal clutch. In this build stronger clutch gears were used. However, this design did not get past functionality testing for failures.
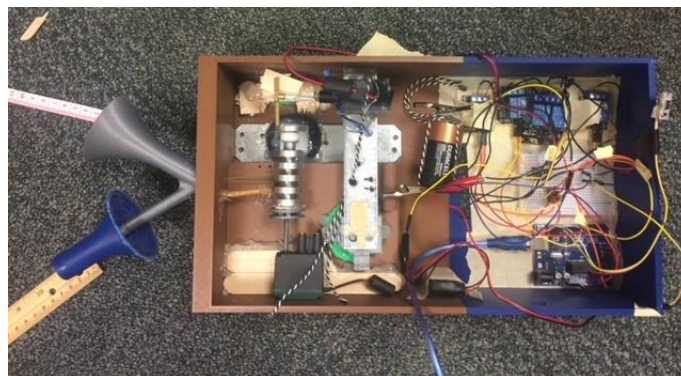
Figure 6; *contents: Prototype 4*

Phase V: Use of Existing Resources

After this, an attempt to motorize and recycle the use of a fishing reel (Figure 7) as the required locking mechanism was tried. The locking mechanism is needed to test the proper operation of the release system.

Figure 7; *contents: Fishing reel for Prototype 5*

Phase VI: Redesign for Robustness

In this phase, the ratcheting gear and pawl system was built. This system used one geared motor to lower and retract a pawl from a ratcheting gear connected to both the spindle holding the tethers of the two pieces of the satellite and a DC motor. To test the reliability and repeatability of this prototype (Figure 8) the ratcheting-pawl system was tested five hundred times.

Figure 8; *contents: Prototype 6*

Corrections were made as needed. The initial distance between the sections of the satellite was measured when the parts of the satellite were still together, and tension was on the spring. To trigger the locking mechanism and begin separation, a cover was placed over the distance sensor, which communicated to the system that an object was near and the mechanical dodge should begin. After separation, the distance the pieces of the prototype parted was measured, and then the cover on the sensor was removed to trigger the reintegration process. To measure the separation distances, a pair of calipers were set up in a fixed position over the span between the pieces of the satellite so the separating piece could be referenced along a more constant scale (Figure 9).
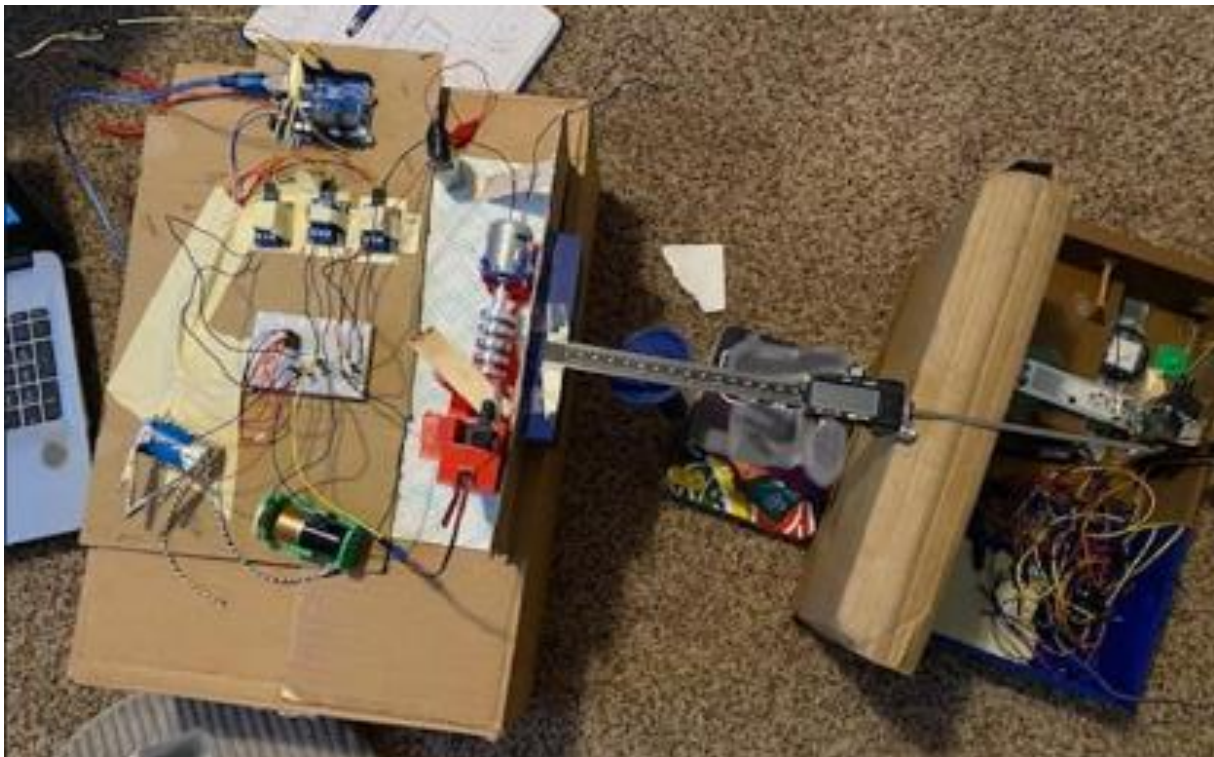
Figure 9; *contents: Prototype 6 test setup*

When the pieces returned to their original positions, the process was repeated. If the system did not complete the course of action properly, the reason for failure was documented and, if needed, the system was manually reset to an average initial position.

Phase VII: Addressing Friction
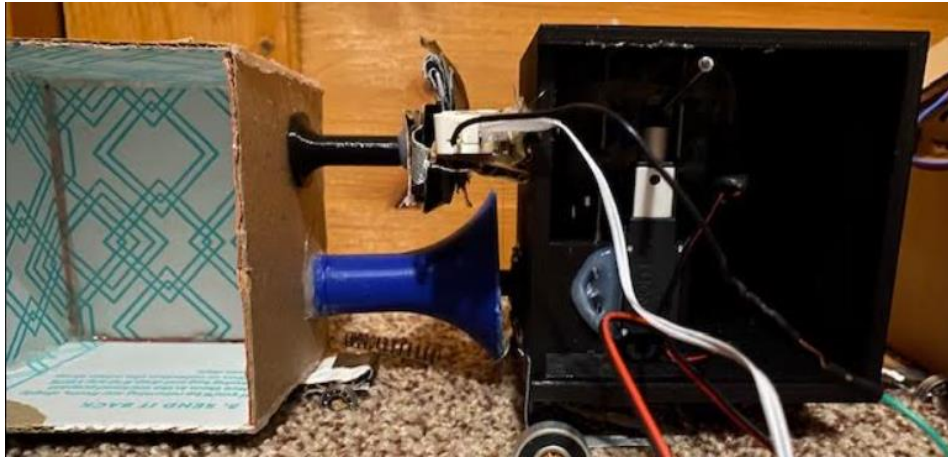
Figure 10; *contents: Prototype 7*

The seventh phase of prototype (Figure 10) was designed to minimize friction in the tether spindle when the pieces of the satellite were supposed to be separating. It involved using a linear actuator to slide a geared motor in and out of contact of a simple fork-type gear connected to the otherwise mostly free-standing tether spindle supported by ball bearings. One of the design goals was to have the spindle be as free standing and free spinning as possible, hence the only constant attachment of the spindle to the ball bearings. To test this prototype (Figure 11),

Figure 11; *contents: Prototype 7 test setup*

three ball bearings were installed on each half of the prototype as wheels in an attempt to observe separation with less friction. The prototype was set up alongside a meter stick so that it would separate approximately parallel to the edge of the meter stick. The IR sensor used as a simple range finder. A white box was placed in front of the sensor to trigger separation after the initial positions of both halves were recorded. After the halves separated, the final positions of both

halves were recorded using the same edge of the satellite halves as was used to record the initial measurement. During reintegration, the target box was moved to control separation after the reintegration was complete. Both successes and any failures to complete the entirety of the task were recorded.

Sensor Development

Initially, sensing an incoming object started out with a LiDAR sensor and a simple algorithm to determine if anything was detected by the sensor within a certain threshold. However, in space, it is important to be able to understand if objects are on a collision path with the satellite of interest. This could be done using a trilateration algorithm for trajectory prediction. In initial testing for the trajectory prediction sensing system, three infrared (IR) sensors were adhered to a triangle with known leg lengths (Figure 12).

Figure 12; *contents: IR sensor triangle*

Using the dimensions of this triangle and the data inputs from the sensors, an algorithm calculated trilateration equations to assign a three-dimensional coordinate to any object within all three sensors' range. This was done by solving three sphere equations for x, y, and z, as shown below,

$$x = \frac{r_1^2 - r_2^2 + x_2^2}{2x_2}$$

$$y = \frac{r_1^2 - r_3^2 + x_3^2 + y_3^2 - (2x_3 x)}{2y_3}$$

$$z = \sqrt{r_1^2 - x^2 - y^2}$$

(Cotera et al, 2016)

where the subscripts of 1, 2, and 3 correspond to the three sensors, "r" signifies the distance reading of the whichever sensor its subscript denotes, x, y, and z with subscripts correspond to the distances the sensors are set apart from each other, and x, y, and z without subscripts become the variables of the three-dimensional coordinate (Cotera et al, 2016). After a set amount of time (such as 50 milliseconds), the sensors would take a secondary measurement and a second three-dimensional coordinate was assigned to the incoming object. With the two coordinates, the algorithm calculated the anticipated third coordinate of the object when it reached the surface of the satellite, assuming the object was traveling linearly. This was done by solving for "t,"

$t = -z_1 / (z_2 - z_1)$

where "t" is a variable, z_1 is equal to the z coordinate of the initially calculated coordinate, and z_2 is equal to the z coordinate of the second calculated coordinate. This "t" was then plugged into the following equations to solve for a future x and y coordinate, denoted as x_3 and y_3, with "x" relating to x coordinates and "y" relating to y coordinates, a subscript of "1" relating to the first set of coordinates calculated, and a subscript of "2" relating to the second set of coordinates:

$x_3 = x_1 + t (x_2 - x_1)$

$y_3 = y_1 + t (y_2 - y_1)$

If x_3 and y_3 are less than the predetermined coordinates that define the dimensions of the satellite, then the satellite should execute a mechanical maneuver. Otherwise, no dodge is necessary.

To test basic functionality of the sensor algorithm performance, a flat white circle was attached to a target stick that could be moved towards or away from the sensor array (Figure 13).

Figure 13; *contents: Sensor target stick*

Sometimes, a larger piece of rectangular paper was attached to increase the detectable surface area of the incoming object. This target was moved in different patterns and speeds toward, away from, or parallel to the sensors to determine if the algorithm could accurately predict a collision within predetermined dimensions that would define the surface of a satellite.

In a test for how small of an object the sensors could register, circles of white copy paper with varying radii were moved toward and away from the sensors via suspension on a taut line leading to the sensors. Once the sensor data from all three sensors was approximately within five centimeters of one another and the circle was the maximum distance from the sensor without compromising this constraint, the distance from the circle to the sensors was measured. Additional tests were conducted to deal with noisy sensors, and to calibrate for ambient conditions.

RESULTS

The results presented in this section are an indication of an improvement over time. The Figure 15 was conducted with only 10 trials per system in Phase III. Figures 16, 17, 46, and 47 represent Phase VI and Phase VII with 504 and 50 trials, respectively. A pie chart was used for the latter two trials to represent the pass/ fail rate.
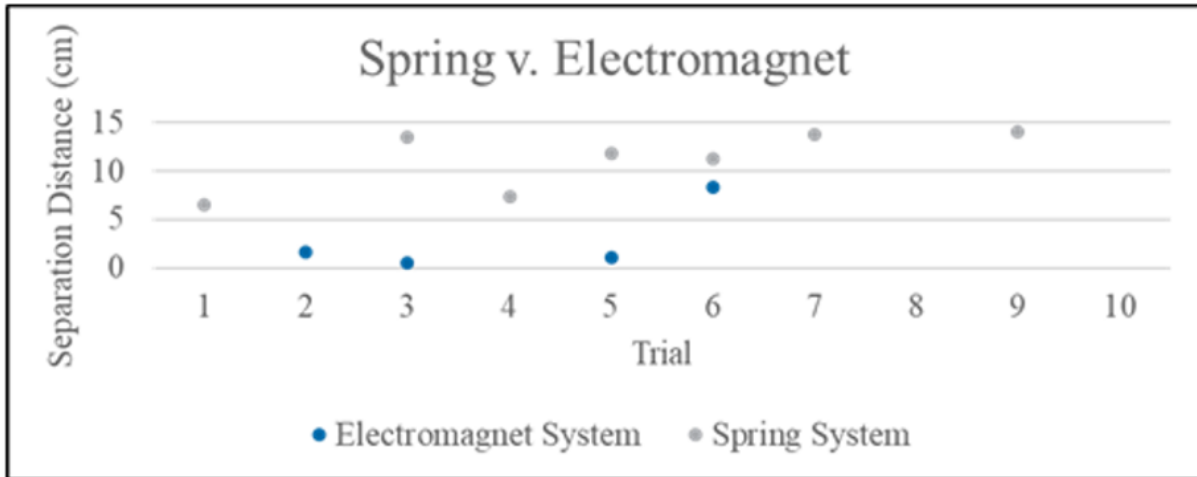
Figure 15: *Comparison of separation distances of "spring" and "electromagnet" with respect to the trial number.*
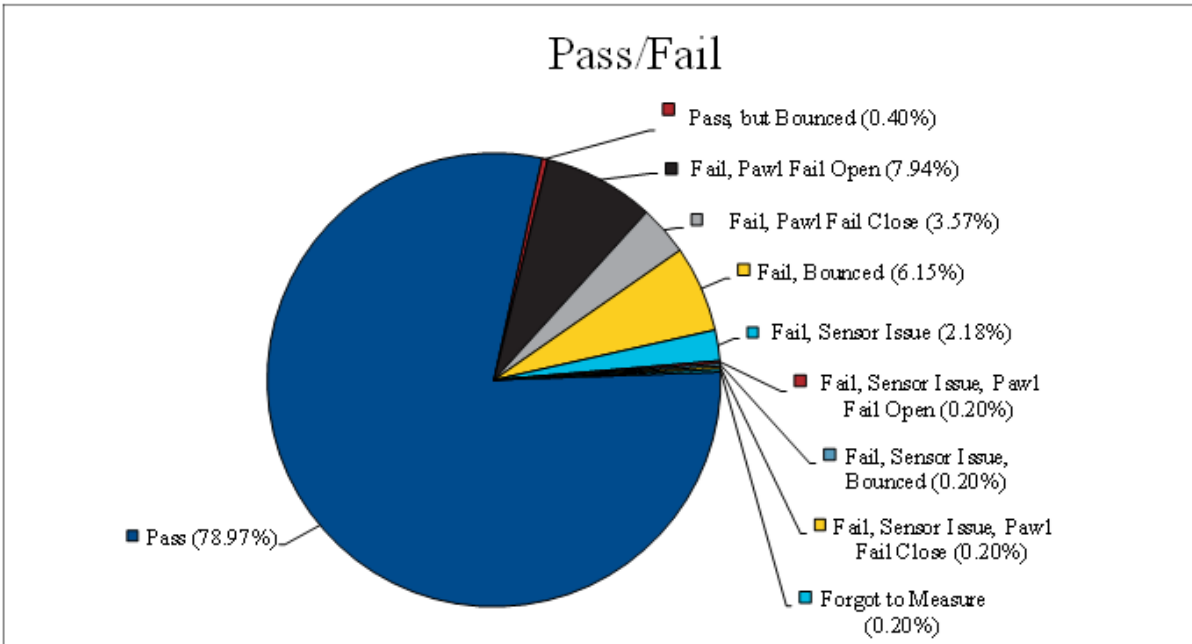
Figure 16: *Prototype 6 Pass/Fail breakdown.*
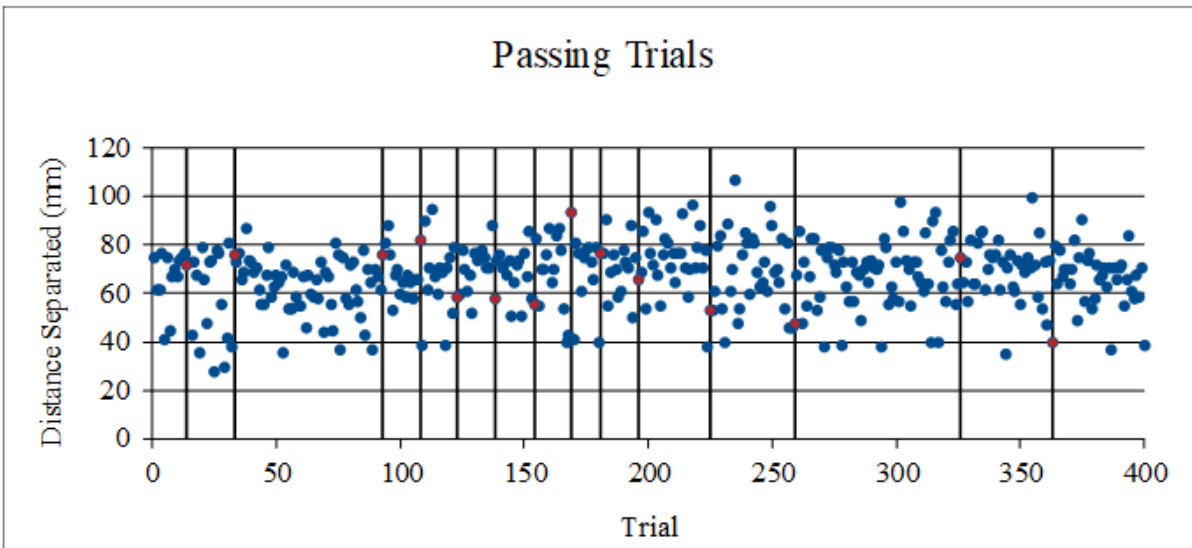
Figure 17: *Prototype 6 Passing separation distances.*
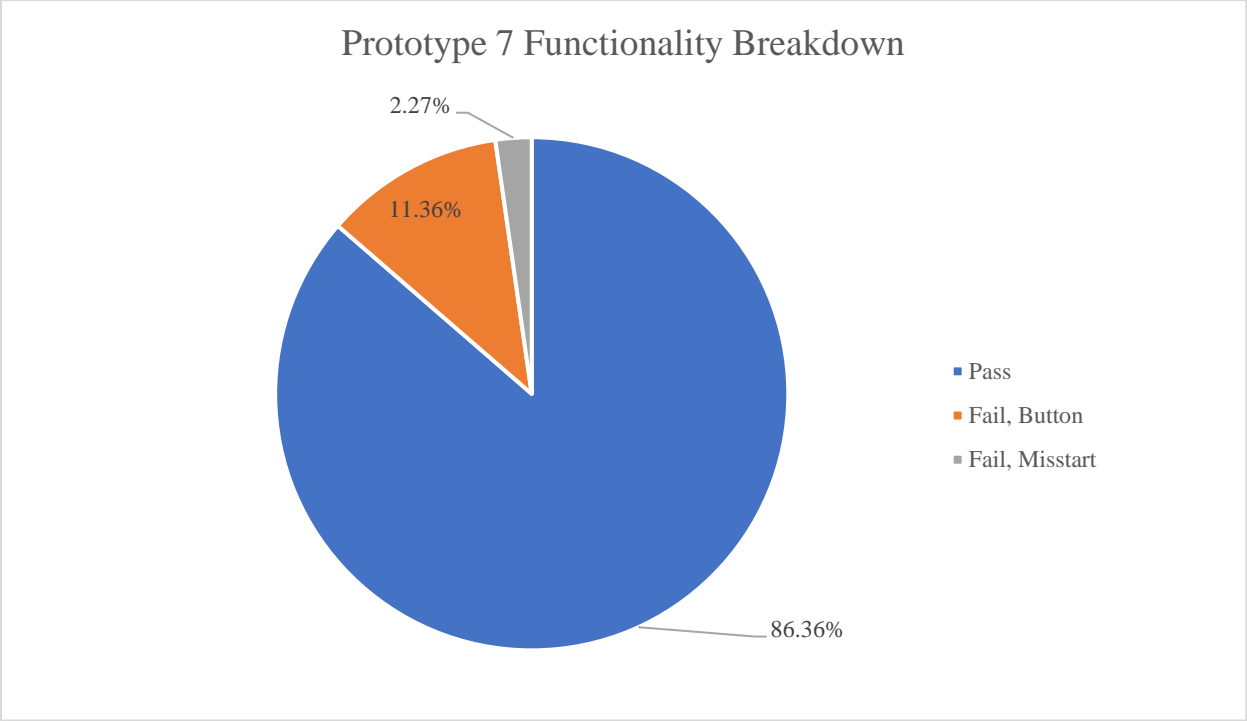
Figure 46; *contents: Prototype 7 Pass/Fail breakdown*
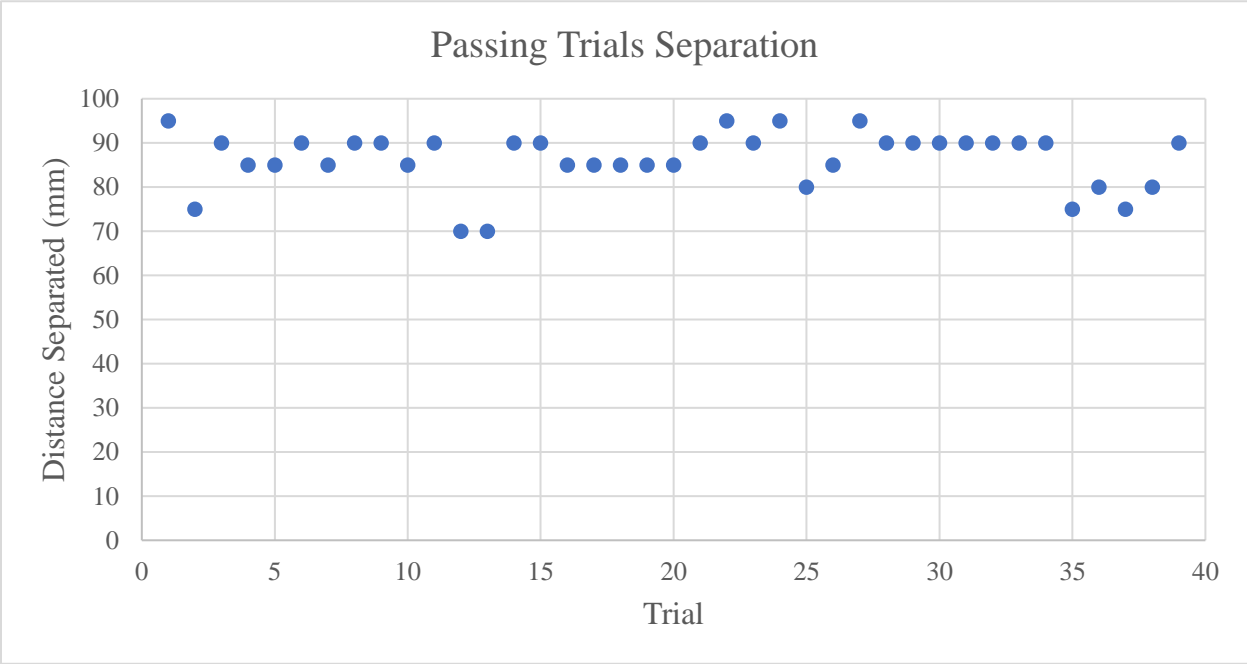
Figure 47; *contents: Prototype 7 separation distances*

In using the infrared sensor, inconsistencies prohibiting the use accurate trajectory prediction algorithms were discovered. To learn more about their sensors and how be to apply them, they were individually calibrated. Also, they were tested in varying lighting environments to ensure that the ambient lighting did not significantly impact sensor outputs. Figures 40 and 41 represent the two sets of calibration curves collected for each of the six sensors, and Figures 43 and 44 represent the results from the ambient lighting testing.
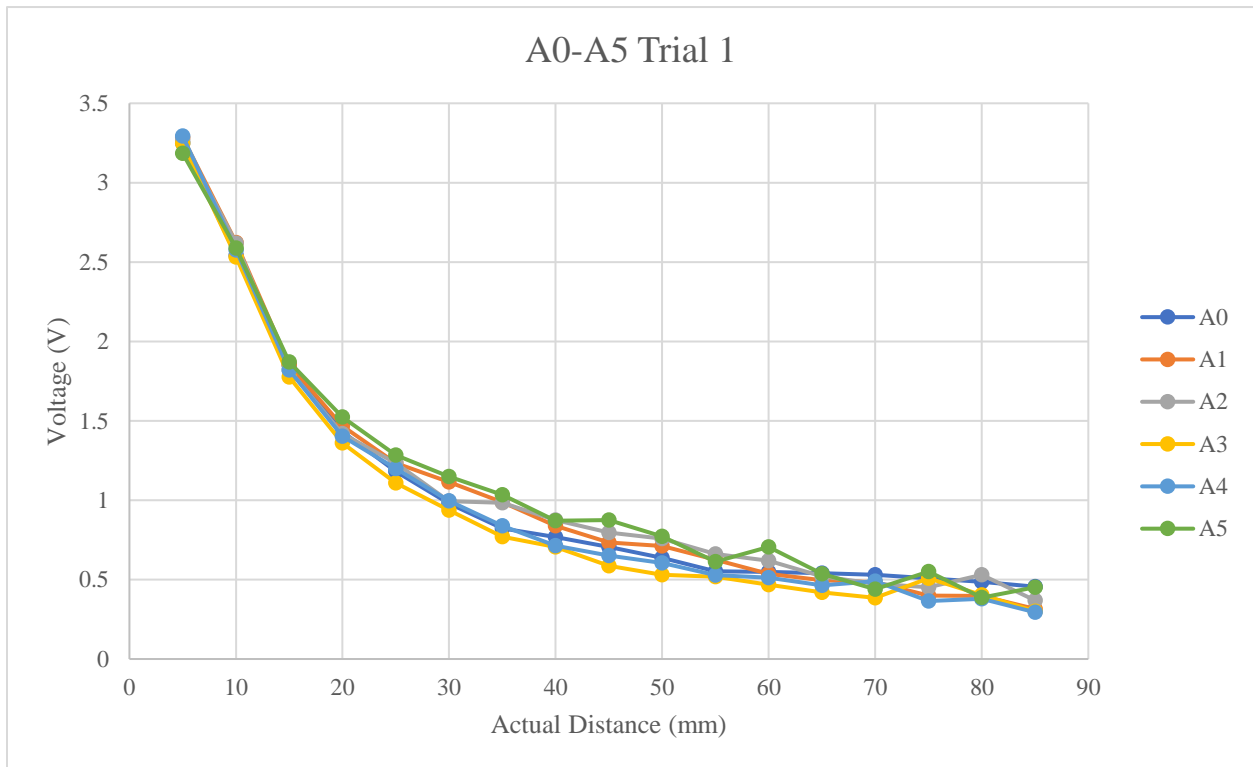
Figure 40: *Averaged voltage outputs for sensors A0-A5 with respect to the actual distance the measurement was taken.*
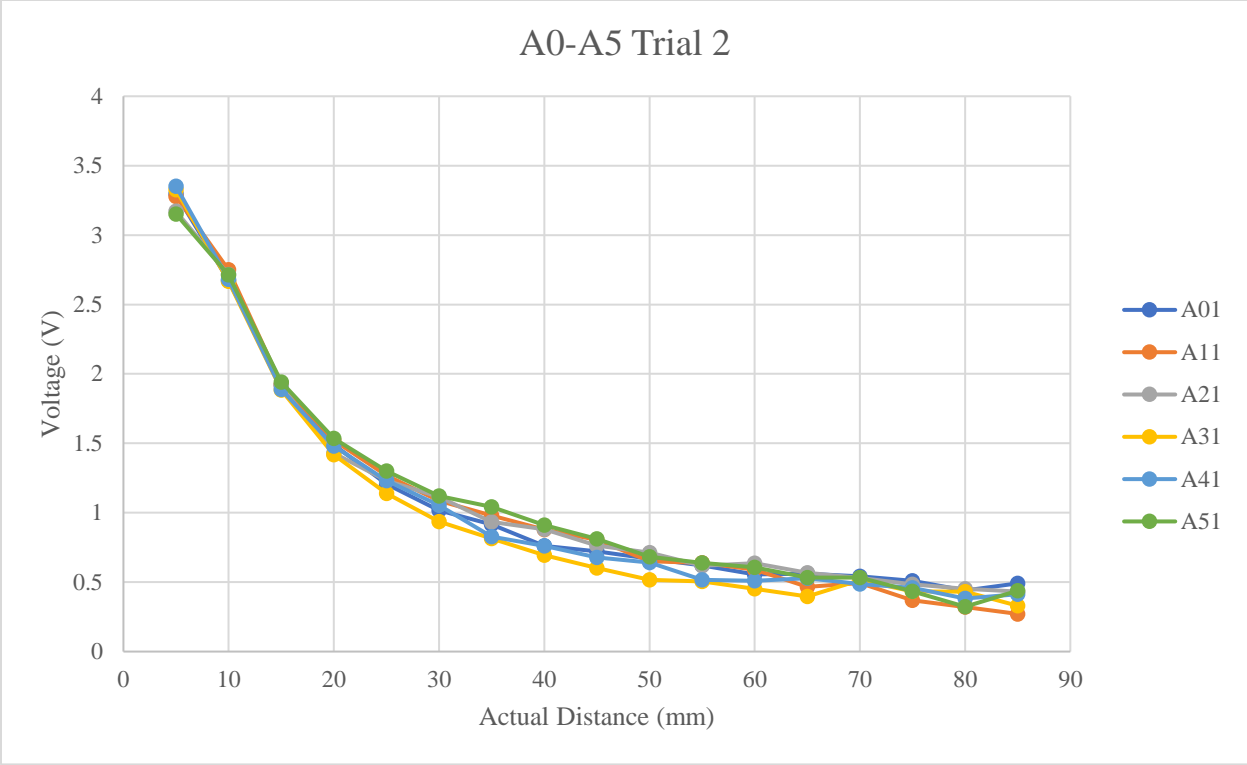
Figure 41: *Averaged voltage outputs for sensors A0-A5 with respect to the actual distance the measurement was taken.*
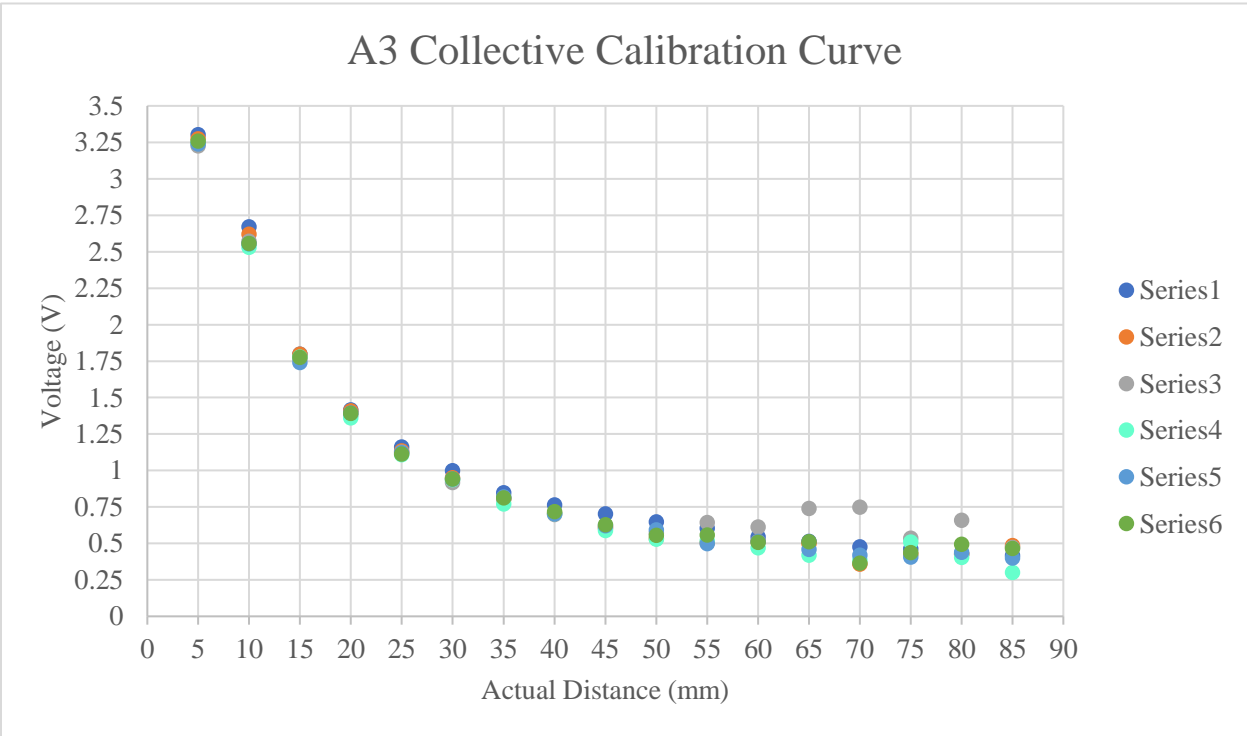
Figure 43: *Averaged voltage outputs for sensor A3 with respect to the actual distance the measurement was taken at in multiple lightings.*
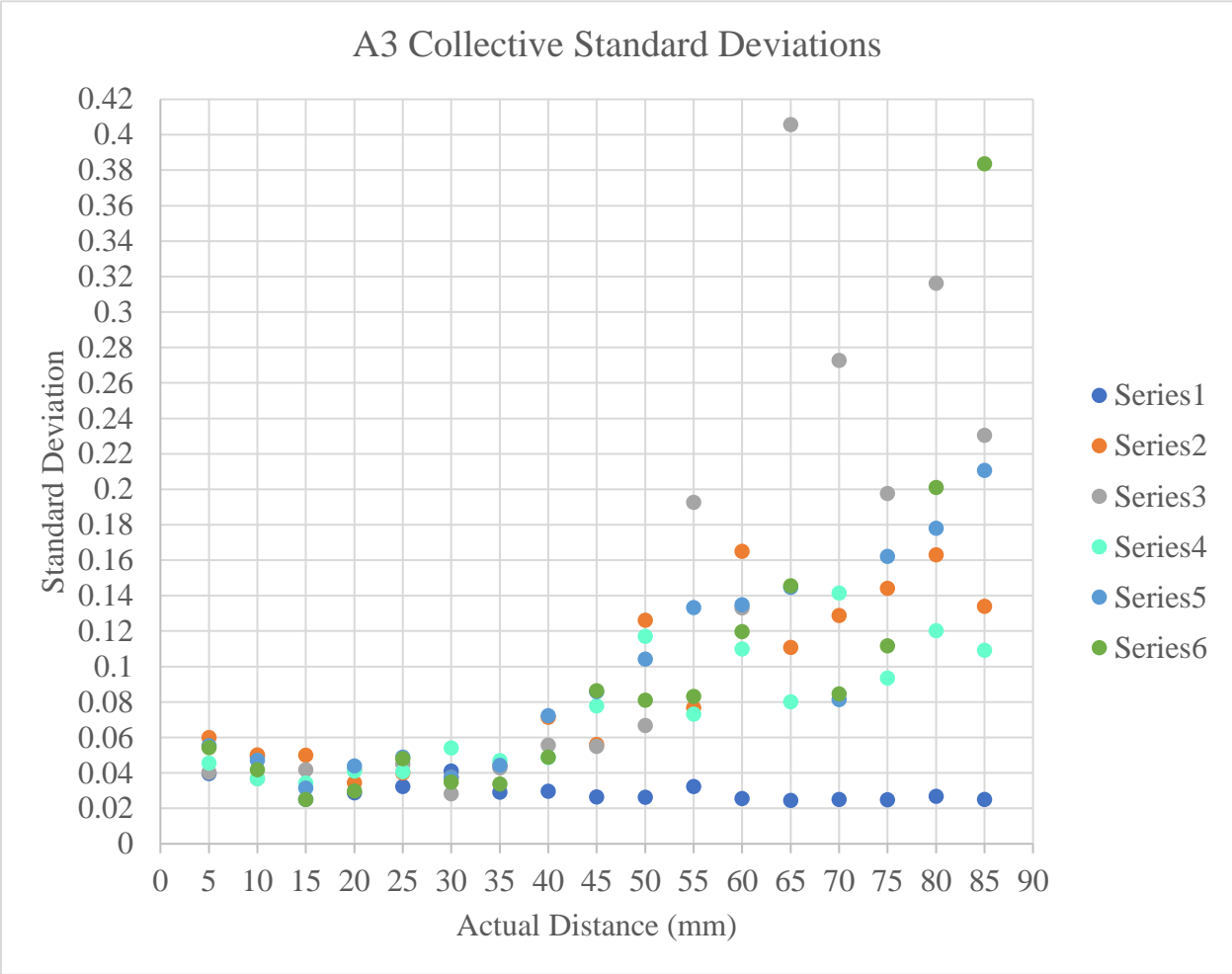
Figure 44: *Standard deviation of averaged voltage outputs for sensor A3 with respect to the actual distance the measurements were taken at in multiple lightings.*

DISCUSSION

In testing the separation mechanism, Figure 15 shows that the spring system (grey) not only completed the maneuver in more trials than the electromagnet system, but it also resulted in farther separations. The standard deviation also shows that the spring system was more consistent, as it has a standard deviation of 3.1 centimeters compared to the 3.6-centimeter standard deviation of the electromagnet system. Most of the electromagnet trials separated less than 11% of the total possible separation distance of the system, while the spring system separated farther on average, with 30% of the spring system trials separating approximately to the maximum separation distance of that setup. Failures of the electromagnet system stemmed from mechanical errors like stripped gears, stiffness in the free spinning spindle, and a detached ball bearing. Spring system failures included misalignments, incomplete spring compression, and mechanical errors like those found in the electromagnet system.

Through testing the ratcheting gear and pawl locking mechanism in 504 trials, the locking mechanism demonstrated a 78.97% pass rate, as shown in Figure 16. For pass/fail tests, a "pass" was considered as the prototype completing the entire cycle of detection, separation, and reintegration without any human intervention beyond placing an object to trigger the sensor and taking measurements. Most of the failures sustained during those trials were results of computer errors, which further demonstrates the potential reliability of the mechanics. However, as shown in Figure 17, the average separation distance was only 67.67 millimeters, with a consistency demonstrated by a 13.3 millimeter (1.33 cm) standard deviation. Each of the vertical lines in Figure 17 with a red data point signifies a change made to the prototype, such as oiling the prototype or tweaking the timing in the computer code. While these changes did not substantially impact the separation distance of the prototype, it did change the pass rates of those trials (Figures 18-32).

Some basic apparent trends in the sensors' and trilateration algorithm's accuracy and limitations have been observed. For example, as more aspects of the algorithm designed to smooth out sensor data were added, the overall accuracy in predicting collisions increased, meaning that what the sensors were outputting was more closely aligned with predictions inferred visually. However, when a series of "if" statements were added to throw out outlier data points caused by an incomplete field of view by only including data within the sensors' range (80

cm) in the averaging algorithm, the accuracy of the algorithm outputs appeared to increase less intensely. Also, detecting a parallel motion seemed more difficult than some of the other motion paths for the algorithm to predict as a non-collision. In attempting to measure velocity, overall consistency rates seemed low, as the time predicted for the incoming object to finish its course in relation to the satellite would be inconsistent, despite trials with relatively similar velocities. The sensors were also only able to register larger objects due to a narrow field of view, as shown in the object size test. The results of this test (Figure 33) should display the sensors' field of view by showing how close a circle of a controlled radii must be to the sensors to get appropriately registered. The larger the circle, the farther away it could be from the sensors, except for the final circle. This last data point may have been an error in experimental setup or measurement. By looking at the distance the circles had to be from the sensor to be registered, the field of view of the sensors could be theoretically calculated, but the results seem too inconsistent to get an accurate estimate. On a larger scale, the algorithm was mainly able to predict collisions, but further improvements to accuracy and expanding the field of view could result in less errors and stronger evidence of proof of concept.

One such attempt to improve accuracy was to calibrate the sensors individually and study the changes in their performances based on changes in ambient lighting. As IR sensors, ambient lighting could change how a sensor would perform as incoming infrared waves from the environment could interfere with the sensor's receiving. The individual calibration curves were collected twice for each sensor, both tests at nighttime, and are shown in Figures 34-39. The relatively small deviation between the two trials seems to suggest that the sensors run approximately consistently when in an approximately consistent environment (like at night with no major lights on other than the computer and those on the Arduino UNO board). Figures 40 and 41seem to demonstrate that the individual calibration curves follow a similar path as evidenced by a similar generic shape of each curve on the graphs, but they are not exact, suggesting that not every sensor performs exactly the same and are thus not entirely interchangeable. While running a similar test with only one sensor at multiple different ambient lighting scenarios, majority of the trials resulted in similarly shaped calibration curves for that sensor (Figure 43). The closeness of these points seems to suggest that for ambient lighting changes between combinations of night, non-direct sunlight, and indoor lighting does not majorly alter the calibration curve. However, the Series 3 trial (grey) in Figure 43 had a slight

variation approximately where the sensor lenses were exposed to direct sunlight (approximately between 60 and 80 mm). While the plots in Figure 43 suggest that the generic calibration curve is approximately consistent across many environments, Figure 44 seems to suggest that the reliability of the sensor outputs are not. Figure 44 shows that as the target gets further from the sensors, the standard deviation between the individual readings (the steadiness of the sensor outputs) increases, thus showing less consistent output and readings indicative of less certain position. Why Series 1 (dark blue) in Figure 44 stays relatively consistent in standard deviation has yet to be determined, but based on the other results, is unlikely to be repeated or relied upon for characterization of that sensor. Figure 44's Series 2, 4, 5, and 6 seem similar as they un-uniformly increase in inconsistency, and ambient lighting in these trials included mixtures between nighttime, daytime, and indoor lighting. In Series 3 (grey), the standard deviation spikes around the time when the lenses are exposed to direct sunlight, suggesting that direct sunlight can also cause more inconsistent readings from the sensor.

The test results of the trials run on Prototype 7 (Figures 45, 46 and 47) demonstrate the pass/ fail rate of the prototype in ability to complete tasks (Figure 45), the breakdown of reasons for failure (Figure 46), and the average separation distance of the trials that passed (Figure 47). As shown in Figure 45, the pass rate of the prototype is approximately 86.36%, about 7.39% higher than the previous prototype, meaning that the prototype appeared to complete the entirety of the detection, separation, and reintegration cycle without any major problems or unassumed human intervention more frequently than the previous prototype. As seen in Figure 46, the main reason for failure was "Button," which means that the prototype failed to wind up close enough to have the tan half of the prototype push a button on the black half to cut power to the motor and thus finishing the cycle (see Figure 10). While the concept of the cycle was still able to be completed without pushing the button as the only thing that changes when the button is pushed is if power is connected to a motor that is usually not moving substantially anyway, it was still regarded as a failure because the prototype did not complete the task. If something of this sort were to happen on a theoretically deployed system, no foreseeable negative impact should occur during that one cycle. While it may seem that the button does nothing, it is there in hopes of preventing over grinding the motor when little to no advances in compressing the spring are to be made. The reason for this failure seemed to stem from the batteries powering the motor running low, and thus they were replaced. Larger batteries may not encounter this lack of power problem

as often, but they were not used in this experiment as a fast and overly strong winding was not needed for ground testing and more power could have led to more damage should a mechanical failure occurred. The other cause of failure, "Misstart" may be less easily preventable but also seems less common.

In Figure 47, the approximate distance that the prototype separated during trials that passed was graphed. A note to make is that the prototype halves sometimes separated at an angle, possibly disturbing the consistency in recording. Based on the recordings, the average separation distance was approximately 86.28 mm, about 18.61 mm higher than the previous prototype, suggesting higher efficiency. Also, the standard deviation of the distances in Figure 47 is approximately 6.46, about 6.84 lower than the previous prototype, also suggesting an improvement in consistency of separation distances. While the measurements taken in Figure 47 are less precise than those for the previous prototype, and while there were 460 less trials in Figure 47 than for the previous prototype, the range of the separation distances seemed to decrease by around 50 mm, further suggesting that prototype 7 is more consistent than its predecessor.

CONCLUSIONS

Overall, the data from the separation system trials demonstrates that using a spring system to separate the pieces of the satellite is more desirable than using an electromagnet system. This is evident in reliability, effectiveness, and consistency demonstrated by the relative success rate, average separation distance, and standard deviation, respectively. This data supports the use of a spring system in order to repel the pieces of a separating satellite. The data collected from the trials run on the ratcheting gear and pawl locking mechanism suggests that it is relatively reliable, especially on a mechanical level. This was shown by the relatively high pass rate and by majority of the failures resulting from timing errors.

The small average separation distance and relatively high standard deviation of those separation distances demonstrates that the ratcheting gear and pawl locking mechanism does not provide the separation system with enough torque to adequately and consistently separate the

pieces of the satellite. For space applications, 67.67 millimeters of separation is most likely insufficient for dodging space debris.

The sensing system still reports errors. More development is needed to improve sensing accuracy. The ability to only detect larger debris is restrictive. This capability is comparable to space debris in sizes that are already detectable from the ground. This limitation defeats the purpose of having an onboard detection system. For ground testing purposes, the sensors seem functional in many situations if each sensor has its own calibration curve and is not exposed to direct sunlight.

The linearly actuated prototype (prototype seven) is more reliable than its six predecessors. This is especially true when the design/system was not running at full potential capacity is considered. Therefore, this generic design, along with some minor improvements could lead to a prototype that is strong, reliable, and effective enough for more complex testing and projections. Though not yet prepared for space application yet, the separating satellite prototype has improved and demonstrated a basic sense of functionality.

Implications for future research into mechanical maneuvers may include incorporating a full prototype, and thus incorporating any nuances with the current linearly actuated prototype and including the electronics piece into the one half of the prototype. This work establishes the foundation for improvement of the trajectory prediction and attempts to further understand the sensors. Finally, more stress testing and minimal gravity simulation testing may add insight on to the design and practices presented in this research.

ACHIEVEMENTS

For years, I have wanted to major in mechanical engineering, but prior to this project, I had not realized the impact of coding into the potentials of the profession. I can see through my trial and error of getting an "accurate" sensing algorithm to run along side my mechanical prototypes, that coding and engineering are not two separate fields, but instead varying intensities of integration.

I have been working on this project for nearly two years. Last year, most of my efforts were on the mechanical/ building side of the project, but this year, more of my effort went into improving the sensing array, a lot of which involved me learning new aspects of C++. When I first came into this project, I had very little coding experience, and that which I did wasn't even in the language I currently use. However, by the end of this school year, I have learned so much in C++, from something as simple as just triggering an electronic relay to initial efforts in compiling a sensor array capable of real-time trajectory predictions and that could be used as a means to improve the situational awareness of a satellite.

ACKNOWLEDGEMENTS

REFERENCES

Denney, J. M., & Upton, E. L. (1994, April 5). *U.S. Patent No. US5300780A*. Retrieved from
https://patents.google.com/patent/US5300780A/en

Commission on Engineering and Technical Systems. (1995). *Orbital debris: A technical
assessment*. Washington, D.C.: National Academies Press.

Cespedosa, F., Garcia, J. L., Lancho, M., & Martinez , L. (2000, May 20). *U.S. Patent No.
US6076467A*. Retrieved from https://patents.google.com/patent/US6076467A/en

Stern, D. P., Peredo, M., & Mendez, J. (Tns.). (2001, November 25). The Space Tether
Experiment. Retrieved July 10, 2019, from https://www-
spof.gsfc.nasa.gov/Education/wtether.html

Mehrholz, D., Leushacke, L., Flury, W., Jehn, R., Klinkrad, H., & Landgraf, M. (2002,
February). Detecting, Tracking and Imaging Space Debris [PDF file]. Retrieved August
26, 2019, from http://www.esa.int/esapub/bulletin/bullet109/chapter16_bul109.pdf

Klinkrad, H. (2010, December 15). Space Debris. *Wiley Online Library*. doi:
10.1002/9780470686652.eae325

Arduino I2C Master Library - UPDATED. (2011, August 7). Retrieved July 18, 2019, from
http://dsscircuits.com/articles/arduino-i2c-master-library#top

Bilimoria, K. D., & Krieger, R. A. (2011, September 27-29). Slot Architecture for Separating
Satellites in Sun- Synchronous Orbits. *AIAA SPACE 2011 Conference & Exposition
[Conference]*, 1. https://doi.org/10.2514/6.2011-7184

Maths Learning Centre UofA. (2013, April 21). EXAMPLE: Finding the equation of a line in 3D
through two points [Video]. YouTube. https://www.youtube.com/watch?v=iqJ9vaPoHkQ

Bellatrix. (2015). Bellatrix Aerospace. Retrieved from
https://www.bellatrixaerospace.com/satellite-propulsion.html

Crisp, N., Smith, K., & Hollingsworth, P. (2015, April 29). Launch and deployment of

distributed small satellite systems [Abstract]. *Acta Astronautica, 114*, 65–78. doi:

10.1016/j.actaastro.2015.04.015

Cotera, P., Veazquez, M., Cruz, D., Medina, L., & Bandala, M. (2016, January 1). Indoor Robot

Positioning Using an Enhanced Trilateration Algorithm. *SAGE journals*.

https://journals.sagepub.com/doi/full/10.5772/63246

Garcia, M. (Eds.). (2017, August 7). Space Debris and Human Spacecraft. Retrieved August 28,

2019, from https://www.nasa.gov/mission_pages/station/news/orbital_debris.html

Thakur, M. (2017, October 1). Arduino 5V relay module KY-019. Retrieved July 17, 2019, from

https://steps2make.com/2017/10/arduino-5v-relay-module-ky-019/

Cofield, C. (2017, December 10). Tiny Space-Debris Detector Will Fly to Station This Week.

Retrieved August 26, 2019, from https://www.space.com/38984-tiny-space-debris-

sensor-to-station.html

MicroElectronicDesign, Inc. (2018). tinyLiDAR Reference Manual [PDF file]. Retrieved July

17, 2019, from https://www.robotshop.com/media/files/pdf/tinylidar-tof-range-finder-

sensor-datasheet.pdf

Esa. (2018, November 1). Analysis and prediction. Retrieved August 26, 2019, from

https://www.esa.int/Our_Activities/Space_Safety/Space_Debris/Analysis_and_prediction

Materials Guide. (2019). Retrieved August 23, 2019, from

https://www.simplify3d.com/support/materials-guide/

MicroElectronicDesign, Inc. (2019). Introducing tinyLiDAR. Retrieved July 8, 2019, from

https://microed.co/tinylidar/

Cavallaro, E. (2019, March 27). Here's How a Fragmenting Satellite Becomes a Debris Cloud.

Retrieved July 10, 2019, from https://futureforce.navylive.dodlive.mil/2019/03/heres-

how-a-fragmenting-satellite-becomes-a-debris-cloud/

Stevenson, D. (2019, April 24). How to Make Electromagnets Repel. Retrieved August 23, 2019,

from https://sciencing.com/make-electromagnets-repel-10053737.html

Hughes, M. (2019, May 08). How Do Time of Flight Sensors (ToF) Work? A Look at ToF 3D
Cameras. Retrieved August 28, 2019, from https://www.allaboutcircuits.com/technical-
articles/how-do-time-of-flight-sensors-work-pmdtechnologies-tof-3D-camera/

Future of Satellites. (2019, October 2). Retrieved July 10, 2019, from
https://www.shapingtomorrow.com/home/alert/3769106-Future-of-Satellites

Koehler, C. (n.d.). BalloonSat: Mission to the Edge of Space [PDF file]. Retrieved August 20,
2019, from
https://digitalcommons.usu.edu/cgi/viewcontent.cgi?article=1947&context=smallsat

The_Technocrat. (n.d.). POWERFUL ELECTROMAGNET (5KG LIFTING). Retrieved July 8
2019, from https://www.instructables.com/id/POWERFUL-ELECTROMAGNET-5KG-
LIFTING/

APPENDIX
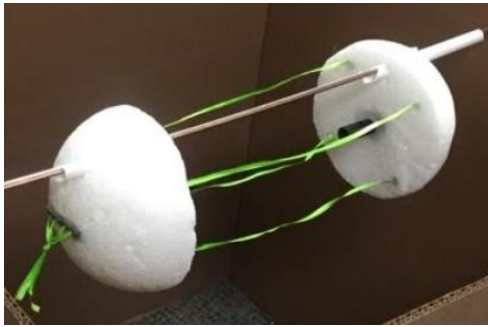
Figure 1: *Prototype 1.*

Figure 2; *contents: Prototype 2*
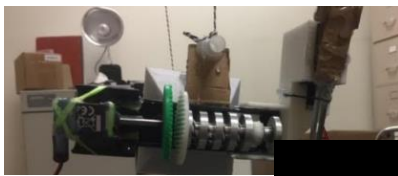
Figure 3; *contents: Prototype 3*

Figure 4; *contents: Electromagnet separating system*

Figure 5; *contents: Spring separating system*

Figure 6; *contents: Prototype 4*

Figure 7; *contents: Fishing reel for Prototype 5*

Figure 8; *contents: Prototype 6*

Figure 9; *contents: Prototype 6 test setup*

Figure 10; *contents: Prototype 7*

Figure 11; *contents: Prototype 7 test setup*

Figure 12; *contents: IR sensor triangle*

Figure 13; *contents: Sensor target stick*

Figure 14; *contents: Example sensor testing setup*
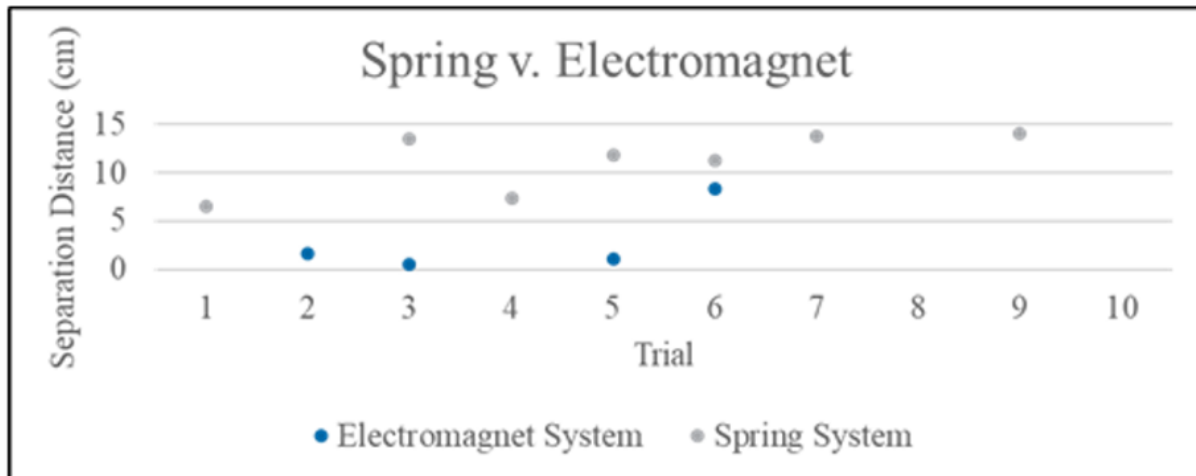
Figure 15; *contents: Comparison of separation distances of "spring" and "electromagnet" with respect to the trial number*
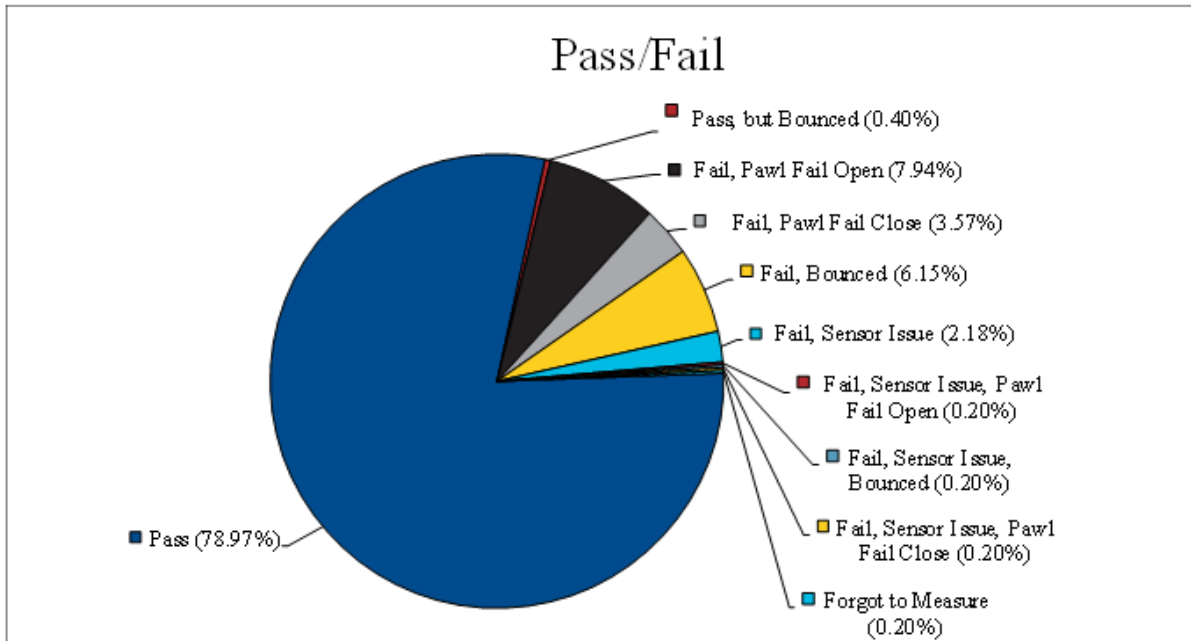
Figure 16: *Prototype 6 Pass/Fail breakdown.*
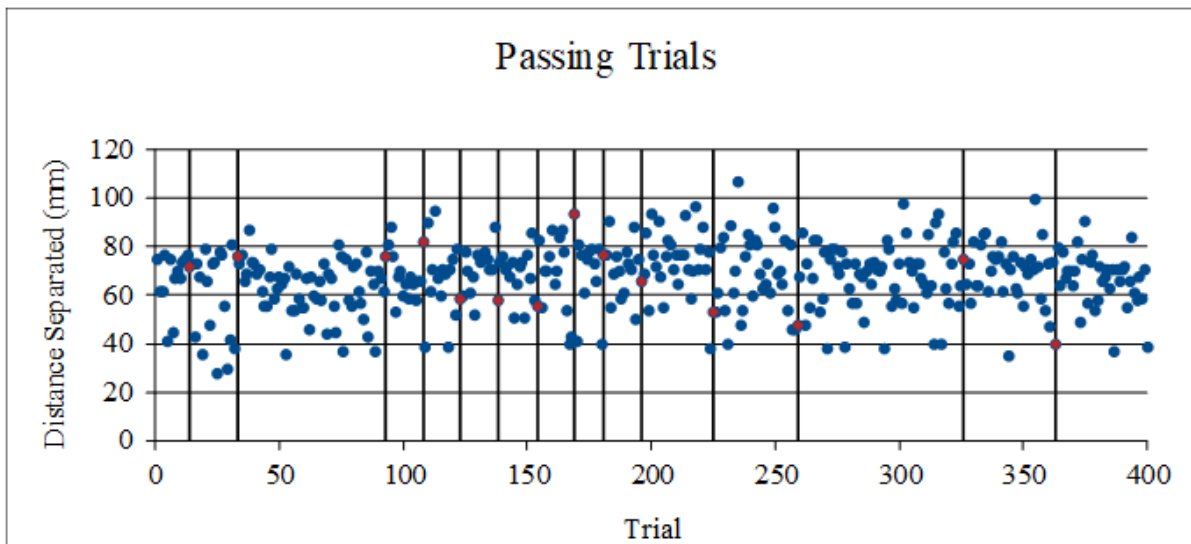
Figure 17: *Prototype 6 Passing separation distances.*

Pass/Fail One

Figure 18; *contents: Prototype 6 Pass/Fail Breakdown*

- Pass (68.42%)
- Fail, Pawl Fail Close (5.26%)
- Fail, Pawl Fail Open (10.53%)
- Fail, Bounced (15.79%)
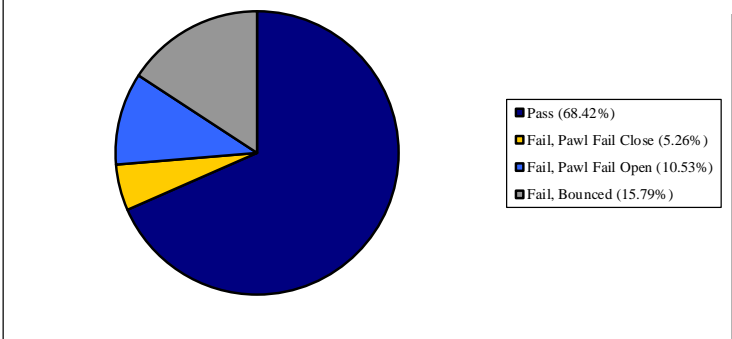
Pass/Fail Two

Figure 19; *contents: Prototype 6 Pass/Fail Breakdown*

- Pass (50.00%)
- Fail, Sensor Issue (5.88%)
- Fail, Pawl Fail Open (14.71%)
- Fail, Bounced (20.59%)
- Fail, Sensor Issue, Pawl Fail Open (2.94%)
- Pass, but Bounced (5.88%)
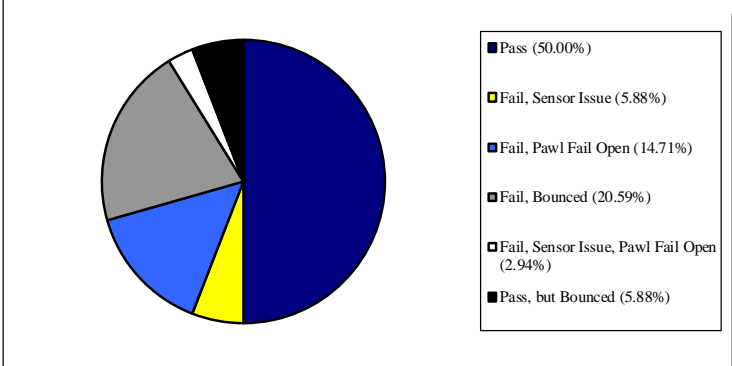
Pass/Fail Three

Figure 20; *contents: Prototype 6 Pass/Fail Breakdown*

- Pass (84.51%)
- Fail, Sensor Issue (2.82%)
- Fail, Pawl Fail Open (11.27)%
- Forgot to Measure (1.41%)
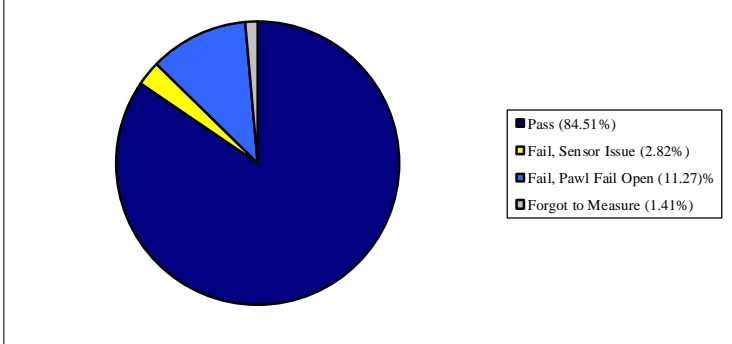
Pass/Fail Four

Figure 21; *contents: Prototype 6 Pass/Fail Breakdown*

■ Pass (75.00%)
■ Fail, Pawl Fail Open (25.00%)
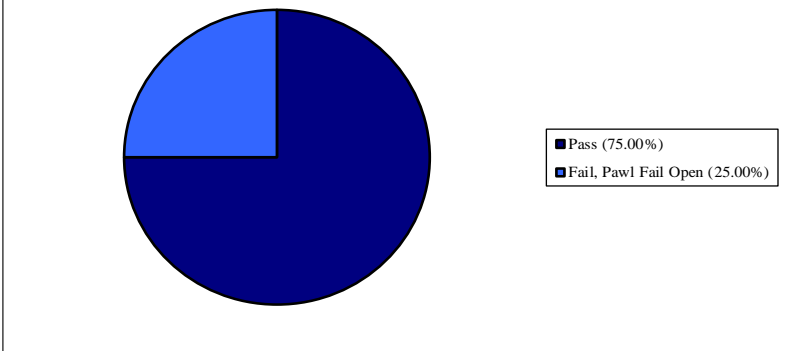
Pass/Fail Five

Figure 22; *contents: Prototype 6 Pass/Fail Breakdown*

■ Pass (75.00%)
■ Fail, Pawl Fail Open (25.00%)
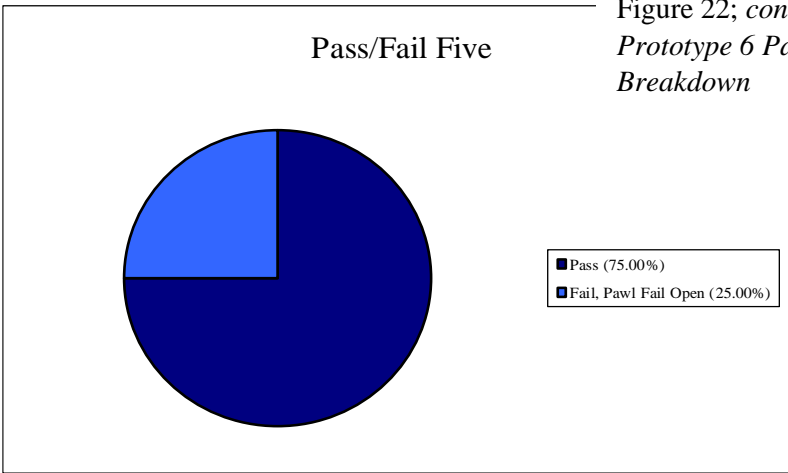
Pass/Fail Six

Figure 23; *contents: Prototype 6 Pass/Fail Breakdown*

■ Pass (75.00%)
■ Fail, Pawl Fail Close (5.00%)
■ Fail, Pawl Fail Open (20.00%)
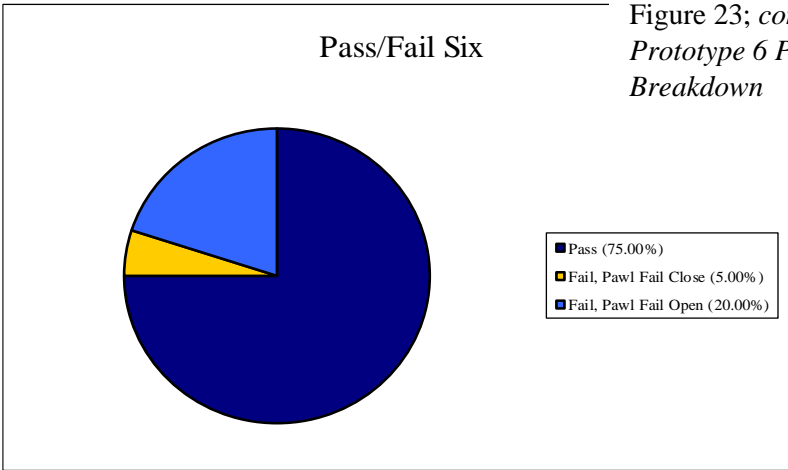
Pass/Fail Seven
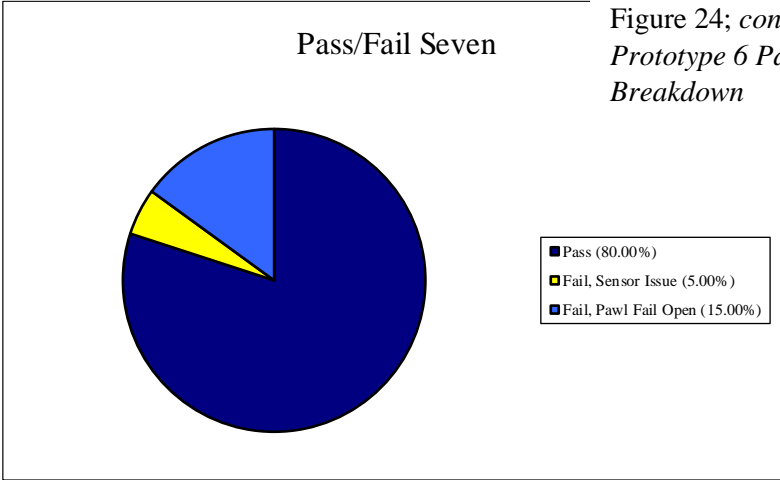
Figure 24; *contents: Prototype 6 Pass/Fail Breakdown*

- Pass (80.00%)
- Fail, Sensor Issue (5.00%)
- Fail, Pawl Fail Open (15.00%)
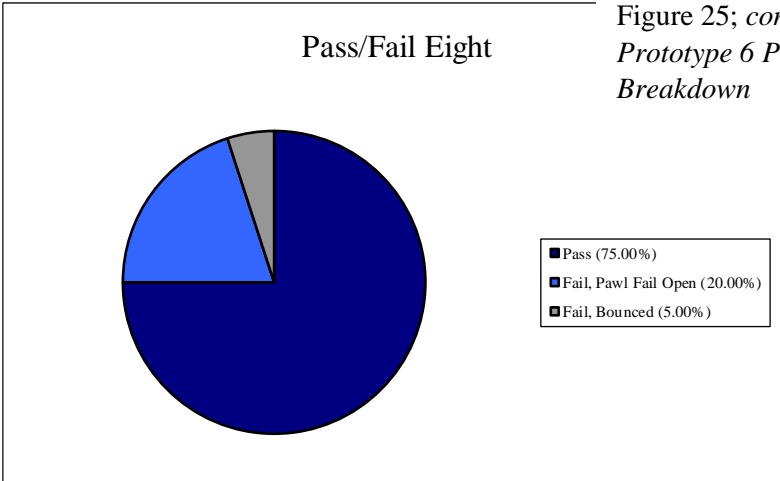
Pass/Fail Eight

Figure 25; *contents: Prototype 6 Pass/Fail Breakdown*

- Pass (75.00%)
- Fail, Pawl Fail Open (20.00%)
- Fail, Bounced (5.00%)

Pass/Fail Nine
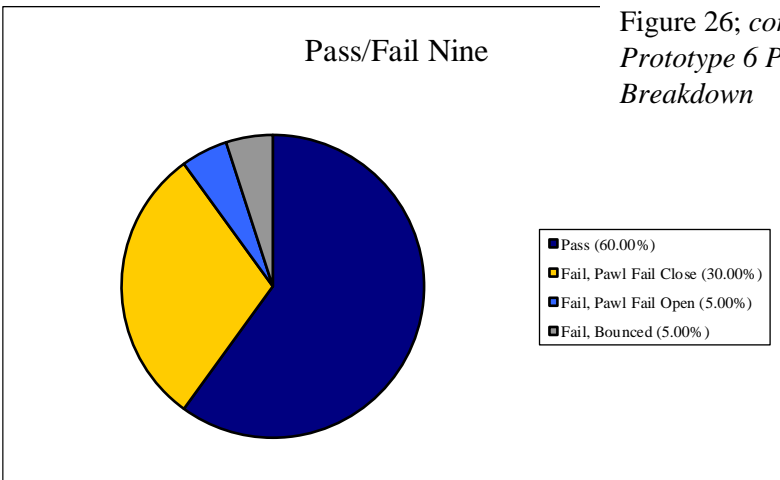
Figure 26; *contents: Prototype 6 Pass/Fail Breakdown*

- Pass (60.00%)
- Fail, Pawl Fail Close (30.00%)
- Fail, Pawl Fail Open (5.00%)
- Fail, Bounced (5.00%)

Pass/Fail Ten

Figure 27; *contents: Prototype 6 Pass/Fail Breakdown*

- Pass (75.00%)
- Fail, Pawl Fail Close (20.00%)
- Fail, Bounced (5.00%)
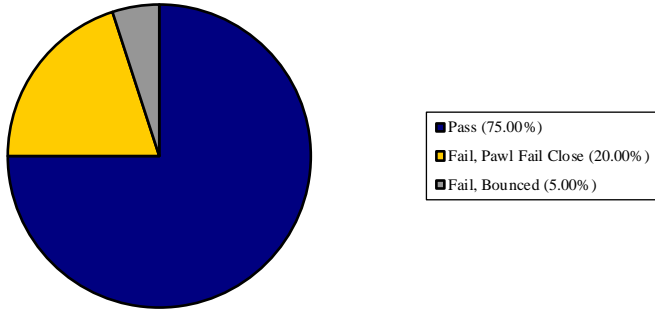
Pass/Fail Eleven

Figure 28; *contents: Prototype 6 Pass/Fail Breakdown*

- Pass (72.5%)
- Fail, Pawl Fail Close (7.50%)
- Fail, Sensor Issue (5.00%)
- Fail, Sensor Issue, Bounced (2.50%)
- Fail, Bounced (10.00%)
- Fail, Sensor Issue, Pawl Fail Close (2.50%)
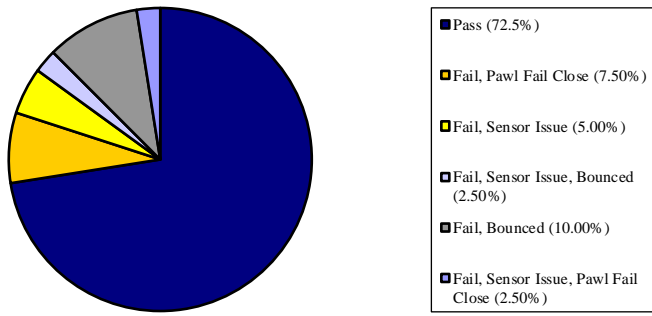
Pass/Fail Twelve

Figure 29; *contents: Prototype 6 Pass/Fail Breakdown*

- Pass (85.00%)
- Fail, Pawl Fail Open (2.50%)
- Fail, Bounced (10.00%)
- Fail, Pawl Fail Close (2.50%)
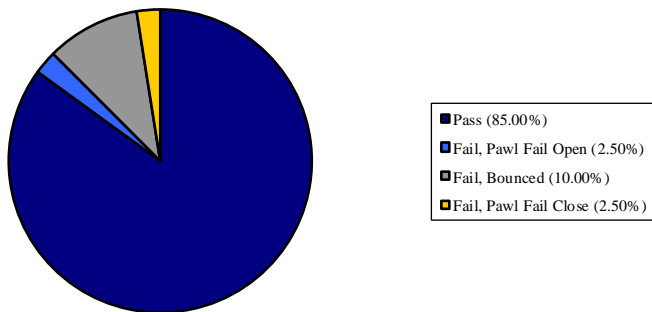
Pass/Fail Thirteen

Figure 30; *contents: Prototype 6 Pass/Fail Breakdown*

- Pass (83.75%)
- Fail, Pawl Fail Close (1.25%)
- Fail, Bounced (10.00%)
- Fail, Pawl Fail Open(1.25%)
- Fail, Sensor Issue (3.75%)
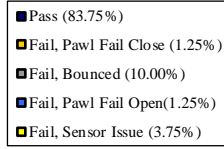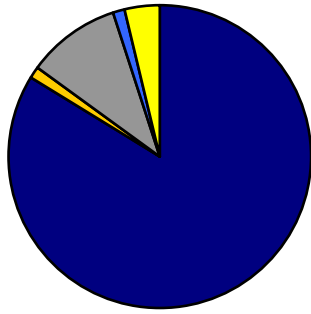
Pass/Fail Fourteen

Figure 31; *contents: Prototype 6 Pass/Fail Breakdown*

- Pass (92.5%)
- Fail, Pawl Fail Close (2.50%)
- Fail, Bounced (5.00%)
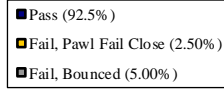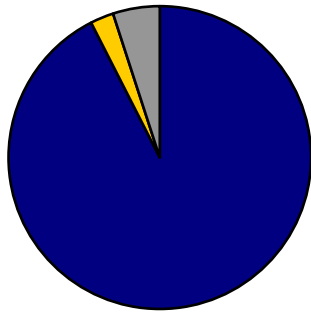
Pass/Fail Fifteen

Figure 32; *contents: Prototype 6 Pass/Fail Breakdown*

- Pass (95.00%)
- Fail, Pawl Fail Open (2.50%)
- Fail, Sensor Issue (2.50%)
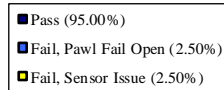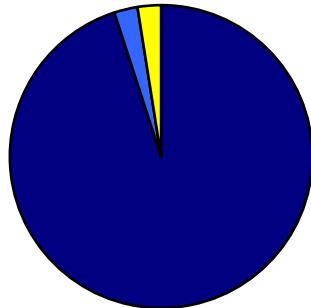
Figure 33; *contents: Distance plotted with respect to the radius of the circle at that distance*
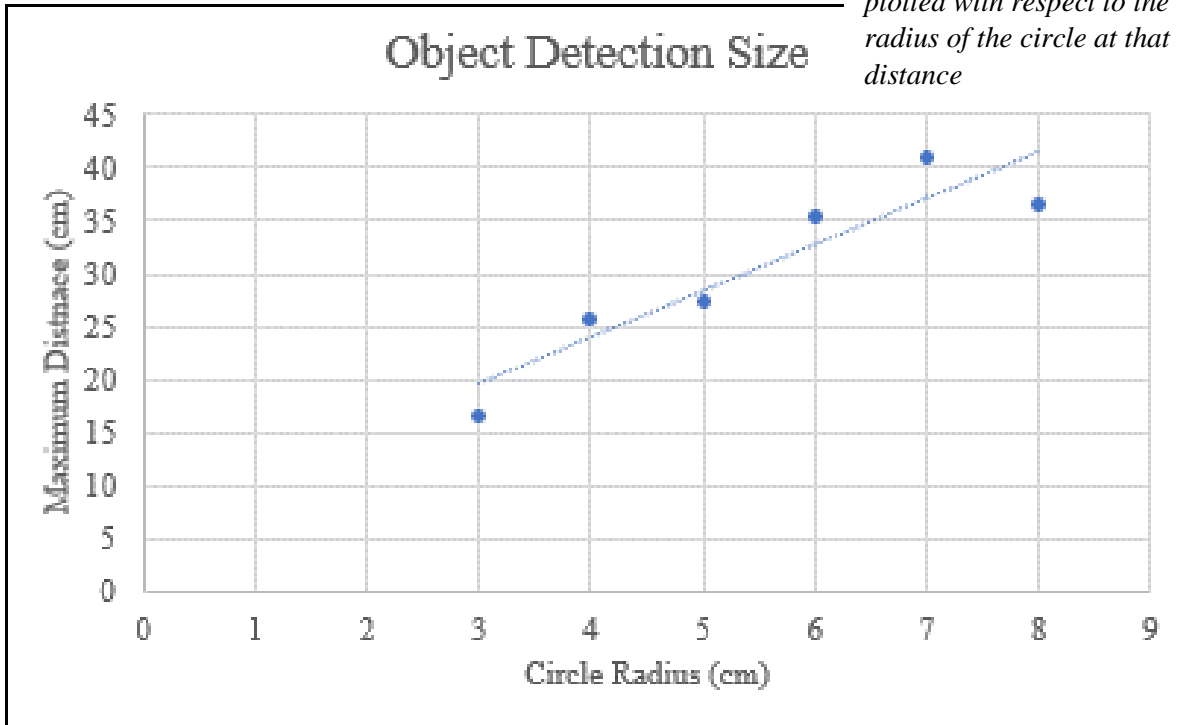
Figure 34; *contents: Averaged voltage outputs for sensor A0 with respect to the actual distance the measurement was taken at*
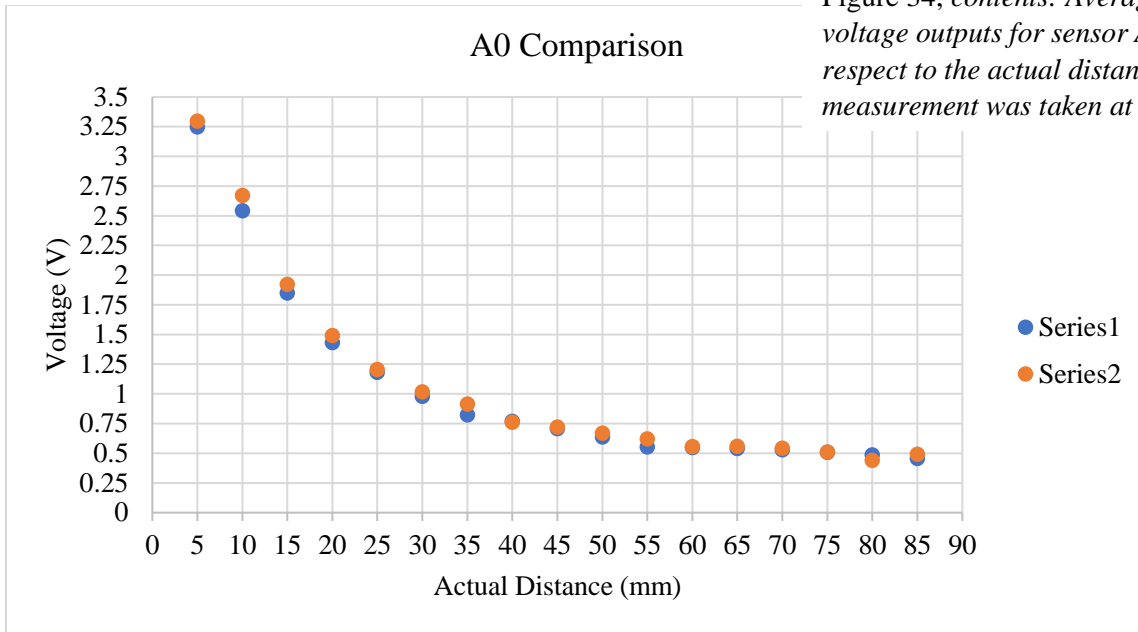
Figure 35; *contents: Averaged voltage outputs for sensor A1 with respect to the actual distance the measurement was taken at*
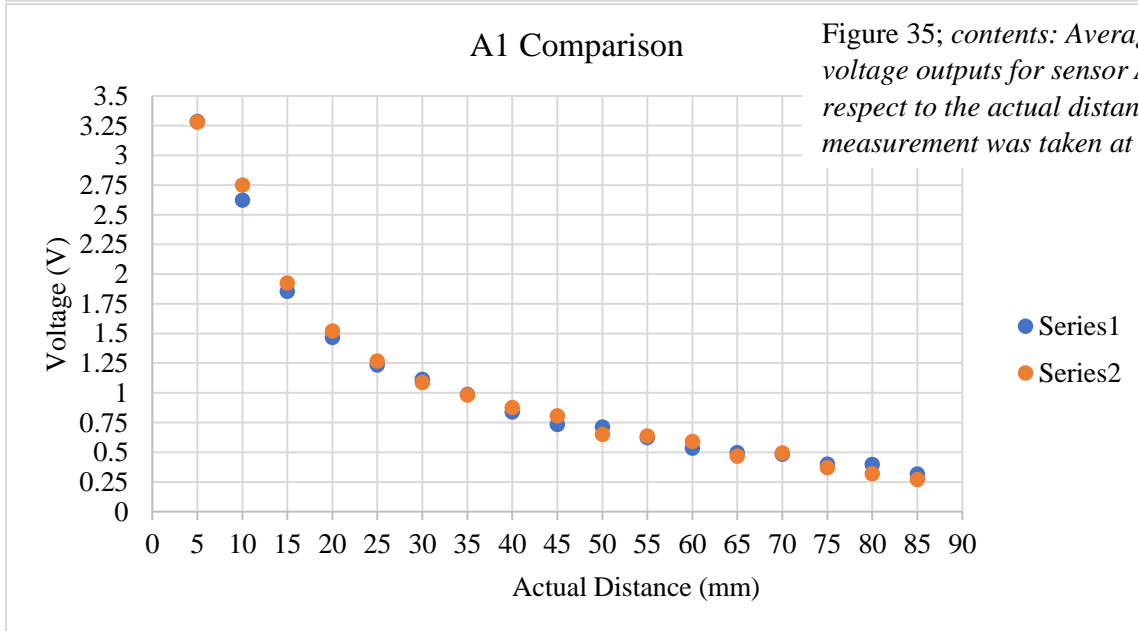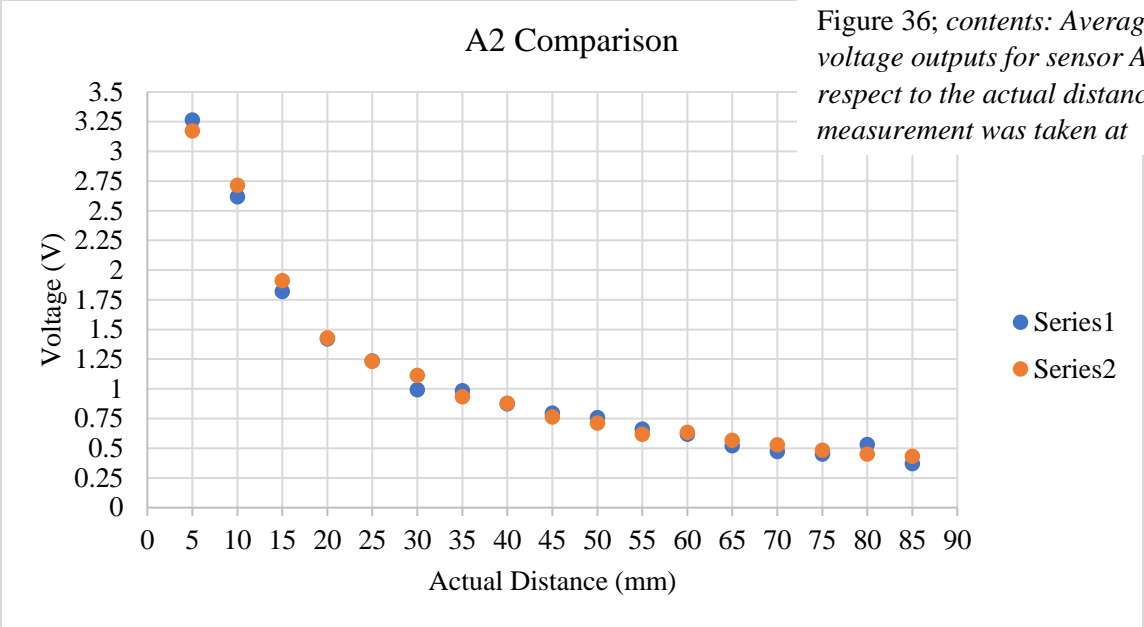
Figure 36; *contents: Averaged voltage outputs for sensor A2 with respect to the actual distance the measurement was taken at*
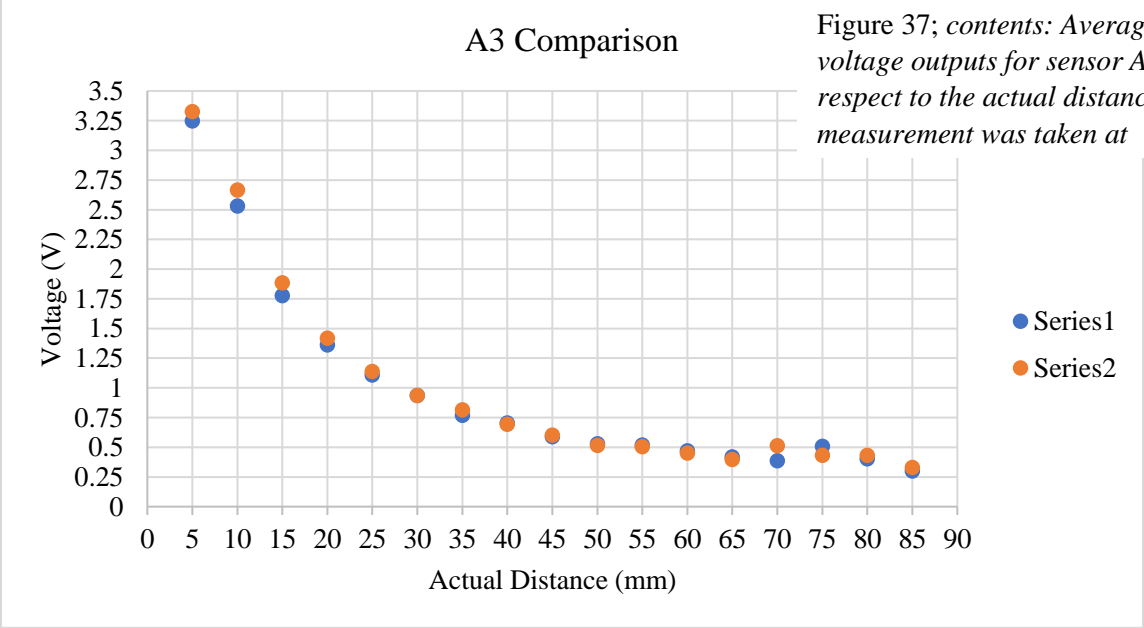
Figure 37; *contents: Averaged voltage outputs for sensor A3 with respect to the actual distance the measurement was taken at*

Figure 38; *contents: Averaged voltage outputs for sensor A4 with respect to the actual distance the measurement was taken at*

Figure 39; *contents: Averaged voltage outputs for sensor A5 with respect to the actual distance the measurement was taken at*
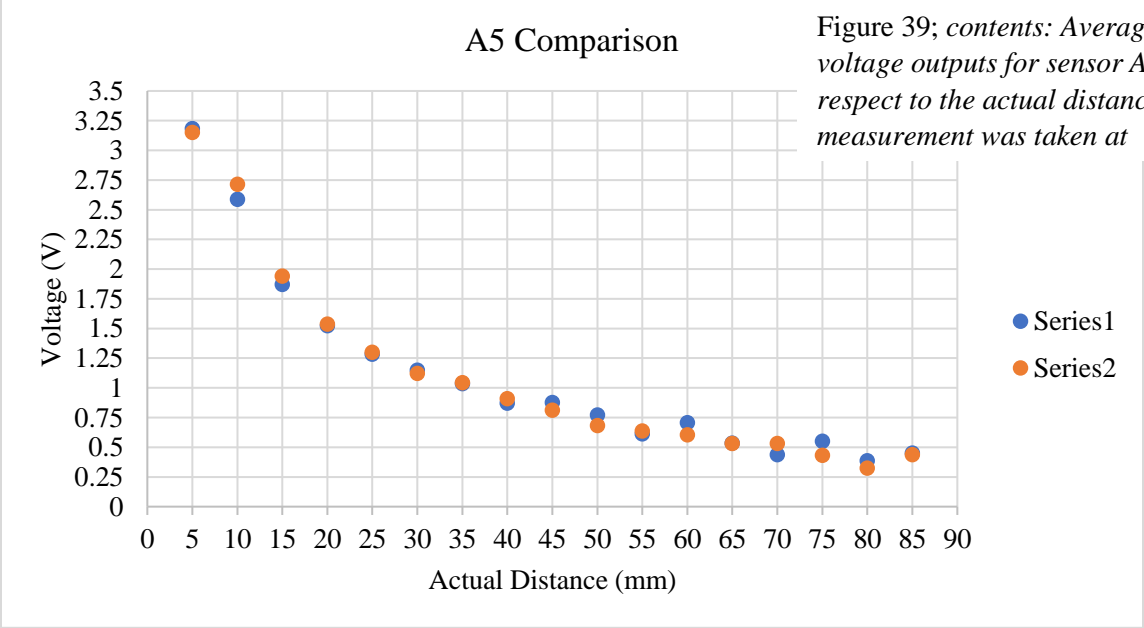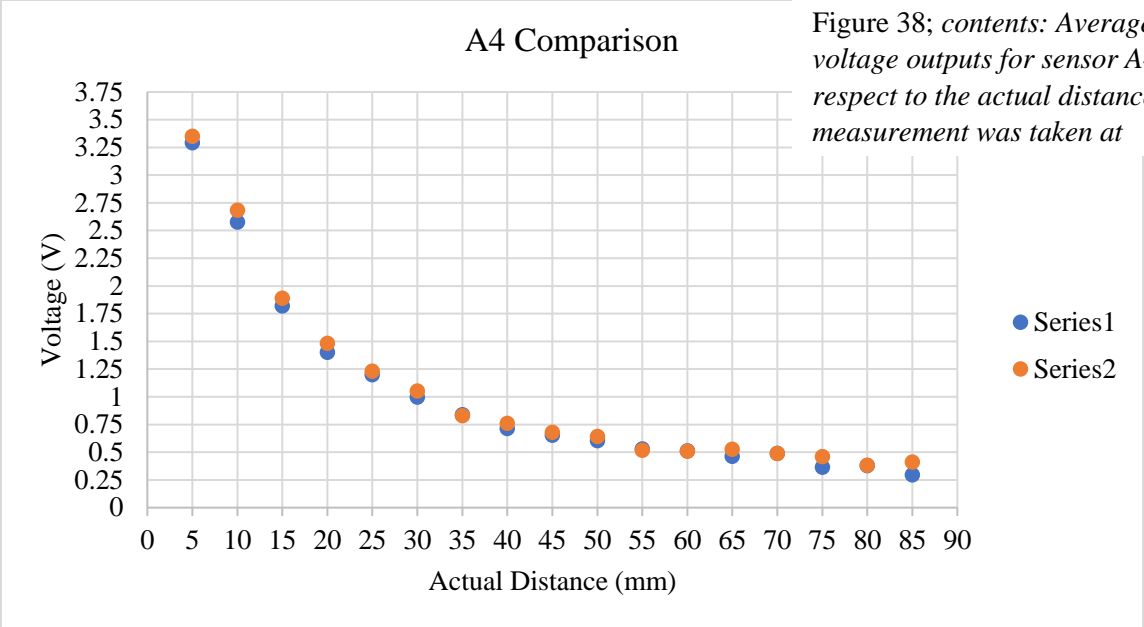
Figure 40; *contents: Averaged voltage outputs for sensors A0-A5 with respect to the actual distance the measurement was taken at*
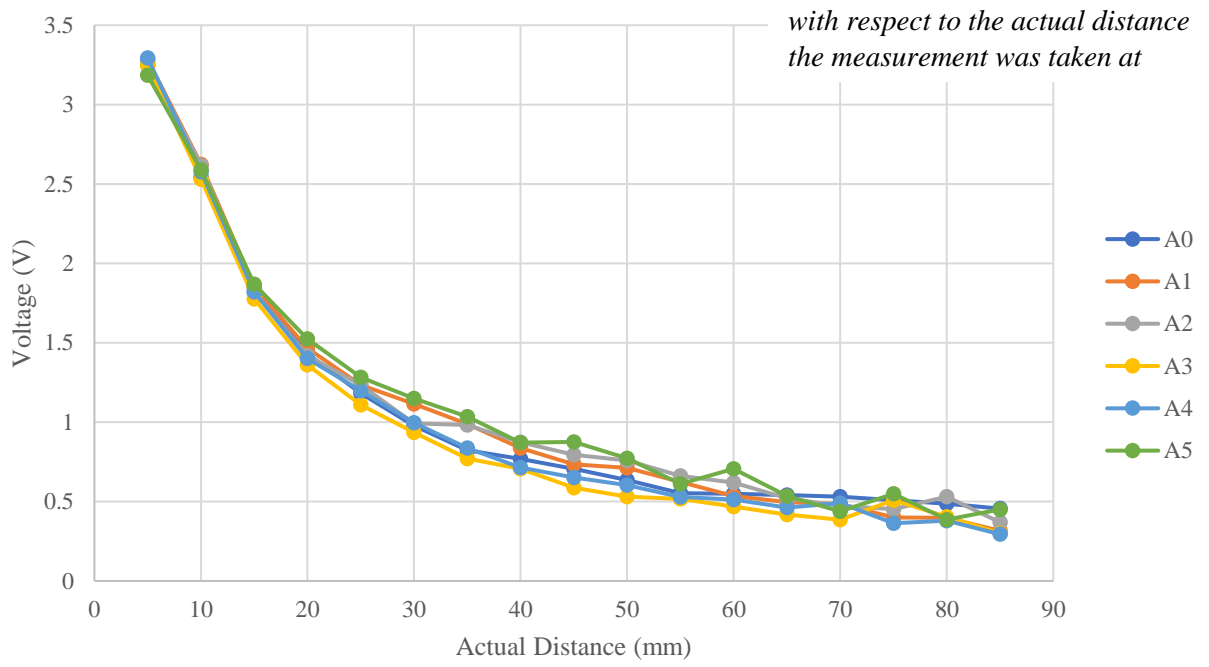
Figure 41; *contents: Averaged voltage outputs for sensors A0-A5 with respect to the actual distance the measurement was taken at*
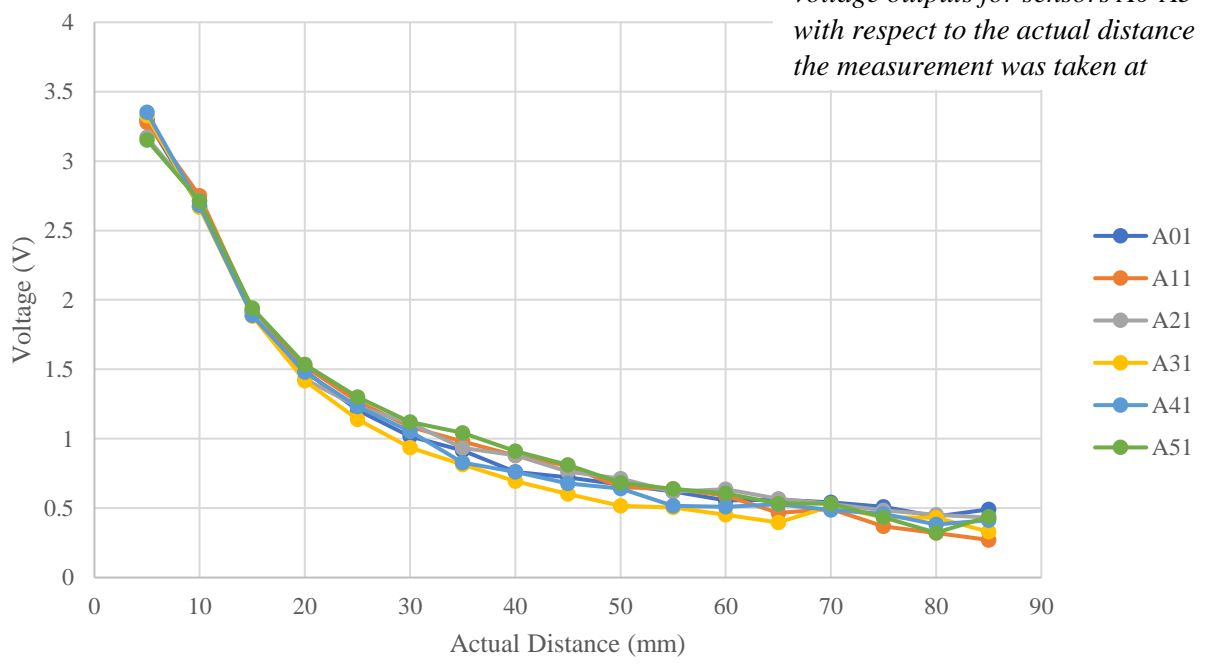
Figure 42; *contents: Standard deviation of voltage outputs for sensors A0-A5 with respect to the actual distance the measurements*
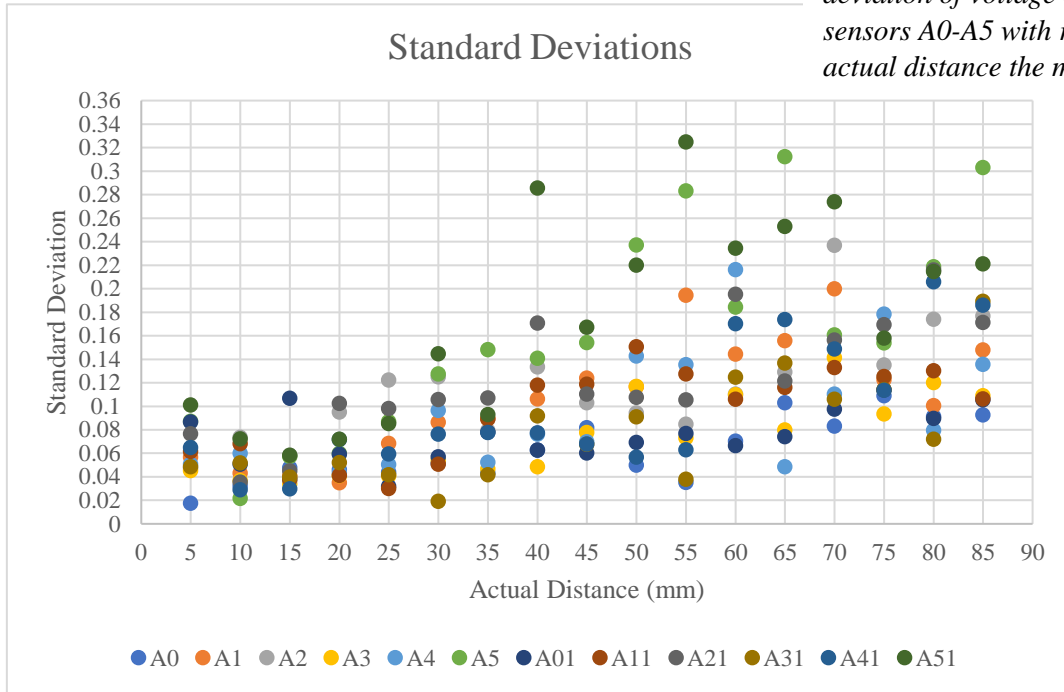
Figure 43; *contents: Averaged voltage outputs for sensor A3 with respect to the actual distance the measurement was taken at in multiple lightings*
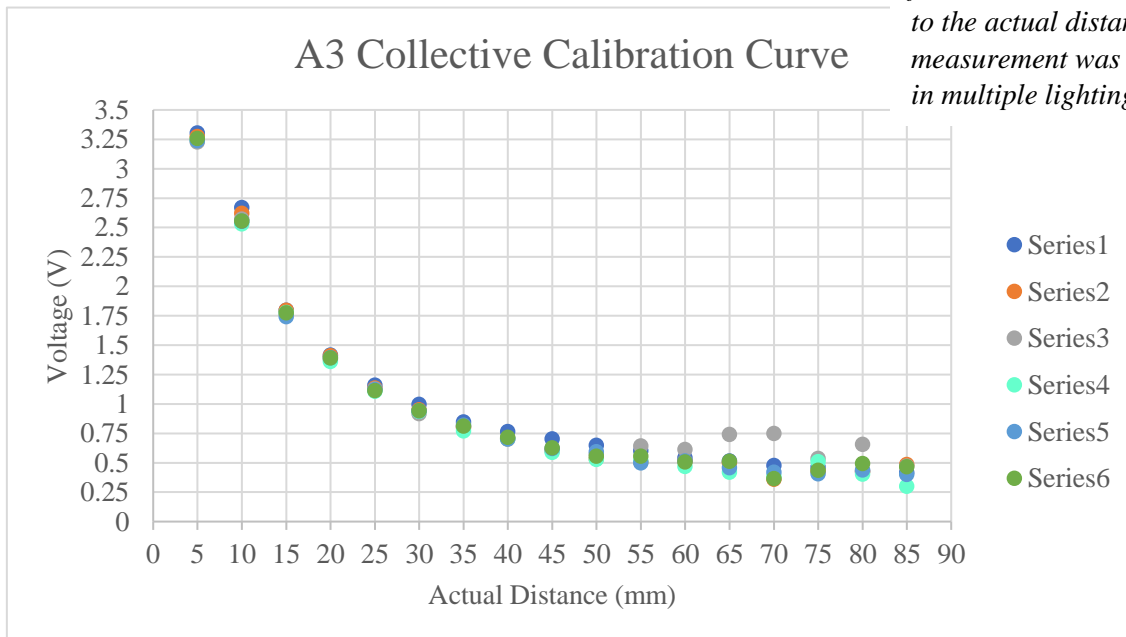
Figure 44; *contents: Standard deviation of averaged voltage outputs for sensor A3 with respect to the actual distance the measurements were taken at in multiple lightings*
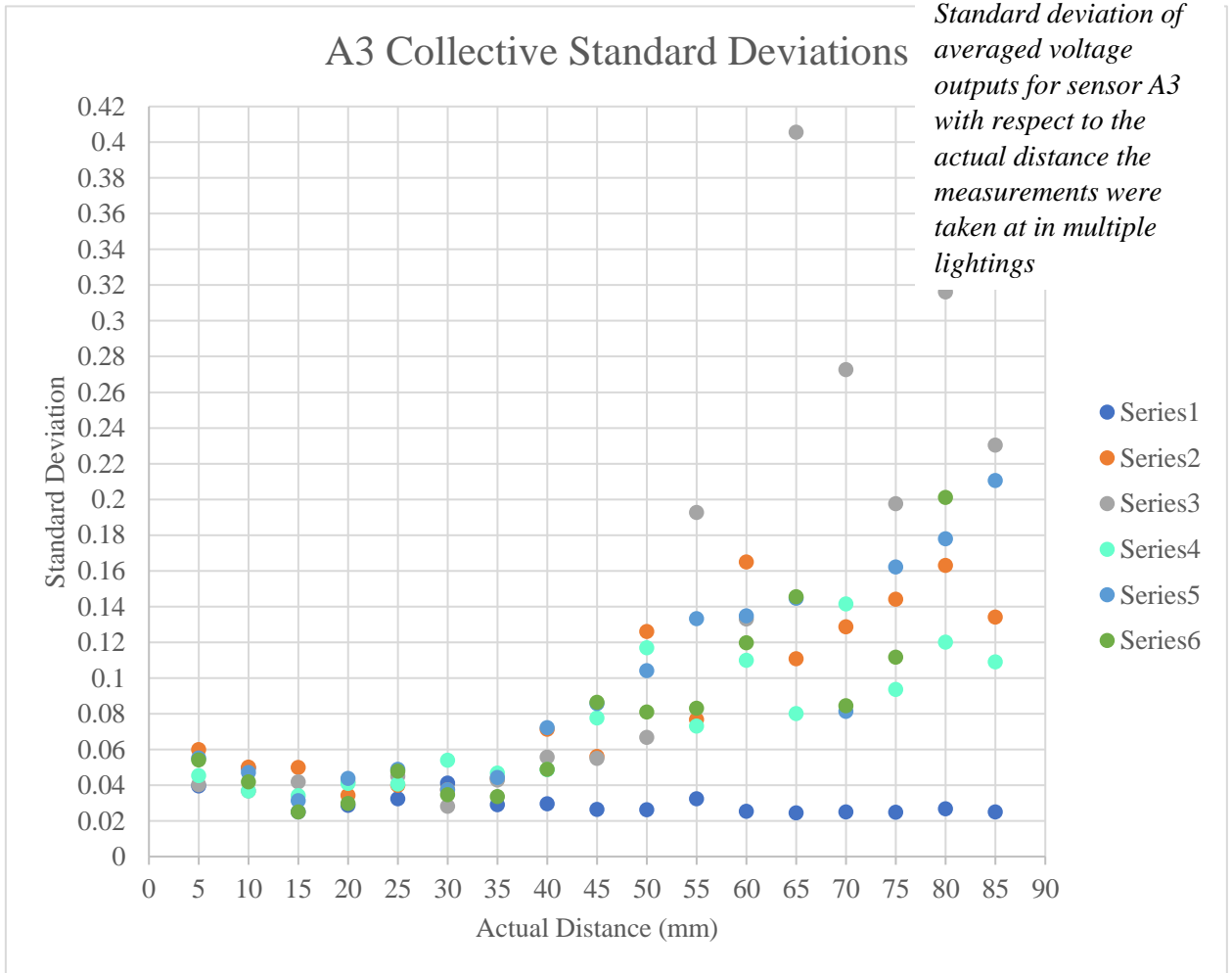
Figure 45; *contents: Prototype 7 Pass/Fail*

Figure 46; *contents: Prototype 7 Pass/Fail breakdown*

Figure 47; *contents: Prototype 7 separation distances*